





# Recent tectonic activity in Central Alborz Mountain, Iran: morphometric analysis and knickpoint identification

Parisa SHOKRI<sup>1</sup>  <https://orcid.org/0000-0002-0763-3789>; e-mail: parisashokry92@gmail.com

Maryam DEHBOZORGI\*<sup>2</sup>  <https://orcid.org/0000-0002-2072-5821>;  e-mail: m\_dehbozorgi@khu.ac.ir

Saeid HAKIMI ASIABAR<sup>2</sup>  <https://orcid.org/0000-0003-3120-4498>; e-mail: saeid.h.asiabar@gmail.com

\*Corresponding author

<sup>1</sup> Department of Earth Science, Kharazmi University, Tehran, 15719-14911, Iran

<sup>2</sup> Department of Geology, Lahijan Branch, Azad University, Gilan, 1616, Iran

**Citation:** Dehbozorgi M, Shokri P, Hakimi Asiabar S (2020) Recent tectonic activity in Central Alborz Mountain, Iran: morphometric analysis and knickpoint identification. *Journal of Mountain Science* 17(12). <https://doi.org/10.1007/s11629-019-5945-2>

© Science Press, Institute of Mountain Hazards and Environment, CAS and Springer-Verlag GmbH Germany, part of Springer Nature 2020

**Abstract:** Alborz, as part of the Alpine-Himalayan orogeny belt, has been the result of the convergence of the Central Iranian and Eurasian plate since the late Triassic. The study area located in Central Alborz encompasses different Quaternary faults. Thus, the present study aimed to evaluate the effect of faults on river landforms through morphotectonic indices and the causes of knickpoints and knickzones in the Bedrock Rivers in part of Central Alborz. To this end, six morphometric indices such as longitudinal gradient (SL), hierarchical anomaly ( $\Delta\alpha$ ), the bifurcation index ( $R$ ), hypsometric integral and hypsometric curve ( $Hi-Hc$ ), relative relief ( $Bh$ ), and basin shape ( $Bs$ ) were calculated and analyzed in 38 sub-basins of the area. Finally, the area was divided into extremely high, high, medium, and low tectonic activity areas using the relative tectonic activity (IAT). Normalized steepness and concavity indices along with the longitudinal profiles of the streams were obtained using Matlab and Arc GIS software. Based on the findings, the existence of slope-break knickpoints at the mountain piedmont at the outlet of large rivers

through active faults demonstrated that most of these landforms were created by movements along the main faults such as Khazar, Nussha, Soheil, Deylaman, Kashachal, representing high tectonic activity in the central and southern parts of the study area. However, the values of these indices were extremely low and indicated low tectonic activity in the northern parts located in the embayment part of the Caspian Sea. Finally, the findings revealed that these classes correspond well to the areas with landforms such as V-shaped and narrow valleys, gorges, deflected and offset streams, deformed Neogene, and Quaternary units that indicate the post-Neogene activity.

**Keywords:** Morphotectonic; Bedrock rivers; Knickpoint; Quaternary Fault; Uplift; Central Alborz

## Introduction

Bedrock Rivers play a significant role in the evolution of mountainous landscapes by controlling the rate of long-term erosion (Hancock et al. 1998; Whipple and Tucker 1999; Whipple 2004). Multiple studies of tectonic geomorphology

**Received:** 23-Jun-2020  
**1st Revised:** 30-Jul-2020  
**2nd Revised:** 31-Aug-2020  
**Accepted:** 14-Sep-2020

demonstrate that bedrock channels can respond to relationships among rock uplift and erosion based on geomorphic indices (e.g., Bull and McFadden 1977; Rockwell et al. 1985; Keller and Pinter 1996; Burbank and Anderson 2001; Schumm et al. 2002; Kirby et al. 2003; Kirby and Whipple 2012). The morphology of the bedrock river is sensitive to tectonic uplift and can be used to define the regional geological evolution (e.g., Seeber and Gornitz, 1983; Keller and Pinter 1996; Kirby and Whipple 2001; Lave and Avouac 2001; Whipple 2004; Perez Pena 2009). In addition, the sensitivity of the river to climate and tectonic changes leads to the quantitative analysis of the degree of the morphology of active deformation (Schumm et al. 2002; Perez Pena 2009). A drainage network displays the correlation between surface processes and structural deformations (Burbank and Anderson 2001). Therefore, analyzing drainage systems is useful for evaluating the impact of tectonic activity on geomorphic processes and landscape development in tectonically active regions (Jackson et al. 1997; Burbank and Anderson 2001). Active landscape changes in the incision/aggradation behaviour of the rivers are related to climatic and tectonic variations (Bull 1991; Burbank and Pinter 1999). Further, fault activities are especially reflected on the longitudinal profiles of the main streams and the analysis mainly relies on quantities obtained from the longitudinal profile of the river. Furthermore, the locally steep sections of the longitudinal profile (Knickpoints) are considered as the key features interpreting fluvial channels. Additionally, geomorphic markers (e.g., prominent knickpoints) at various elevations and distances from the stream mouth to marine terraces by unsteady and transient river incisions can be used to evaluate uplift and erosion rates. It is noteworthy that knickpoints may be associated with structural features such as faults fractures or other joints or lithology changes. Accordingly, geomorphic studies are important in evaluating earthquake hazards, mainly for areas with recent activities in Holocene and Pliocene-Quaternary (Burbank and Anderson 2001; Schumm 2007; e.g., Kurtz et al. 2018; Sharma et al. 2018). In this study, we aimed to discuss the possible association of anomalously high values of the stream-length gradient index (SL) and Normalized steepness

index ( $K_{sn}$ ) with recent uplift in the Alborz Mountain. Computed values of morphotectonic indices and the results of interpretation of knickpoints also suggest the potential influence of tectonic structures, possibly resulted from the oblique convergence of Arabian and Eurasian plates in the Late Triassic. Therefore, the collision and shortening rate of the Alborz Mountain have recently caused earthquakes and faulting. Considering the above-mentioned explanations, the present study focused on the geomorphic morphology of the rivers in order to identify the effect of active faults on drainage System Rivers in part of Central Alborz.

## 1 Study Area

The study area is located in the Central Alborz of Iran in the south of the Caspian Sea (Figure 1). The Alborz Mountain is considered as an active fold-and-thrust belt which is situated within the broad Arabia-Eurasia collision zone (e.g., Berberian 1983; Rad 1986; Alavi 1996; Axen et al. 2001; Jackson et al. 2002; Allen et al. 2003; e.g. Ritz et al. 2006) resulted from the oblique convergence of Arabian and Eurasian plates in the Late Triassic at the rate of 20-24 mm/yr (Stocklin 1968; Rad 1986; Vernant et al. 2004; Reilinger et al. 2006; Zanchi et al. 2006). In addition, it is mainly developed in the Mesozoic-Cenozoic as a consequence of the closure of the Neo-Tethys Ocean (e.g., Aghanabati 2004). The area includes Mesozoic, Paleozoic, or Proterozoic deposits over thrust Cenozoic deposits in an inversion tectonic-based basin (Zanchi et al. 2006). Paleozoic and Mesozoic faulted and folded rocks, Paleogene volcanic sequences, Neogene and Quaternary deposit along the faults (Baharfiruzi and Shafeii 2005) (Figure 2). The tectonic activity of the Alborz range occurred due to movements at the North of Central Iran and the northwest of the Caspian Basin (Vernant et al. 2004; Ritz et al. 2006). The Alborz region has been affected by regional compression from the end of the Cretaceous to the Pliocene-Recent (Berberian and King 1981; Burk et al. 2013) and the regional stratigraphy indicates the uplift as early Tortonian times (Johnson 1997; Braga et al. 2003). Further, Quaternary kinematics demonstrates the most uplift in Central Alborz

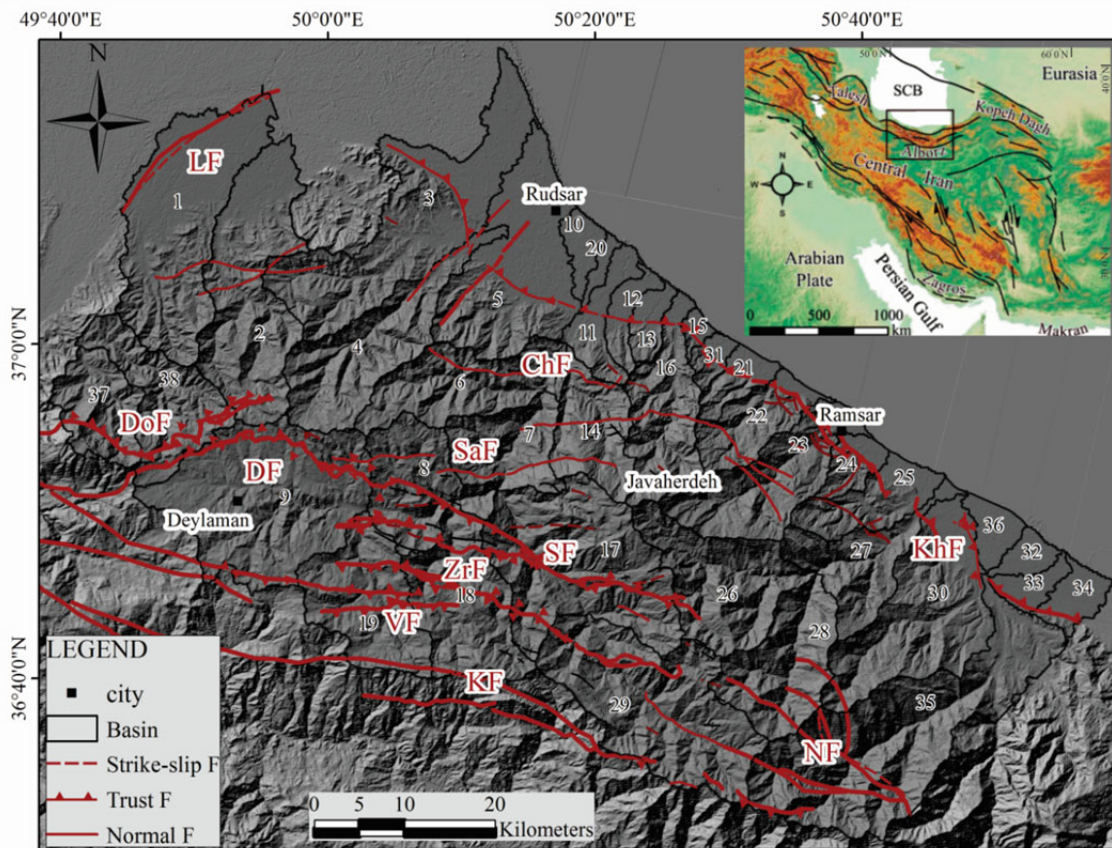


**Figure 1** Location map showing the geologic and tectonic setting of Alborz Mountain range (north Iran). The study area in Central Alborz (Allen 2004) and 38 sub-basins, Main structures and faults in the DEM (Hillshade) used for the morphometric analyses. ZrF = Zarin rajah Fault, VF = Varbon Fault, DF = Deylaman Fault, DoF = Dorfak Fault, KF = Kashachal Fault, SF = Soheil Fault, SaF = Samamus Fault, Chf = Chalmehrud Fault, NF = Nusha Fault, KhF= Khazar Fault, LF = Lahijan Fault.

(Ballato et al. 2013). Therefore, the collision and shortening rate ( $5 \pm 2$  mm/ yr) of the Alborz range have recently caused earthquakes and faulting (Berberian and King 1981; Stampfli et al. 1991; Berberian and Yeats 1999; Vernant et al. 2004). Based on the fault kinematics of the central Alborz, the trend of the folds and thrusts includes left-lateral strike-slip faults trend ENE in the east to a left-lateral strike-slip faulting WNW in the west and oblique reverse movements (Axen et al. 2001; Jackson et al. 2002; Allen et al. 2003). Regarding the Alborz Mountain, seismic and geomorphic studies indicate recent tectonic activity which is important in evaluating earthquake hazards (e.g., Kurtz et al. 2018; Sharma et al. 2018). In the Alborz, seismic records represent a high frequency of earthquakes of a relatively small magnitude (<4) and infrequent large earthquakes (>5.1) (Berberian and Yeats 2001), including the earthquakes of Rudsar and the Gorgan, all of which are influenced

by the activity of the Khazar fault. The active tectonics of the Manjil-Rudbar fault zone was studied due to the existence of several active faults and large-magnitude earthquakes documented in western Alborz. It should be noted that the movement of the active tectonics of Khazar, Nusha, Soheil, Deylaman, Kashachal, Kelishom, Zarrin rajeh, Dorfak, Samamus, Lahijan, Chalmehrud and Varbon faults has caused destructive earthquakes in the area. Accordingly, the current study presented new structural and Pliocene-Quaternary geologic data of the Deylaman and Soheil faults in order to analyze active deformations.

## 2 Method

Morphometric indices can indicate abnormalities in the river system or along with mountain ranges. These anomalies may be related



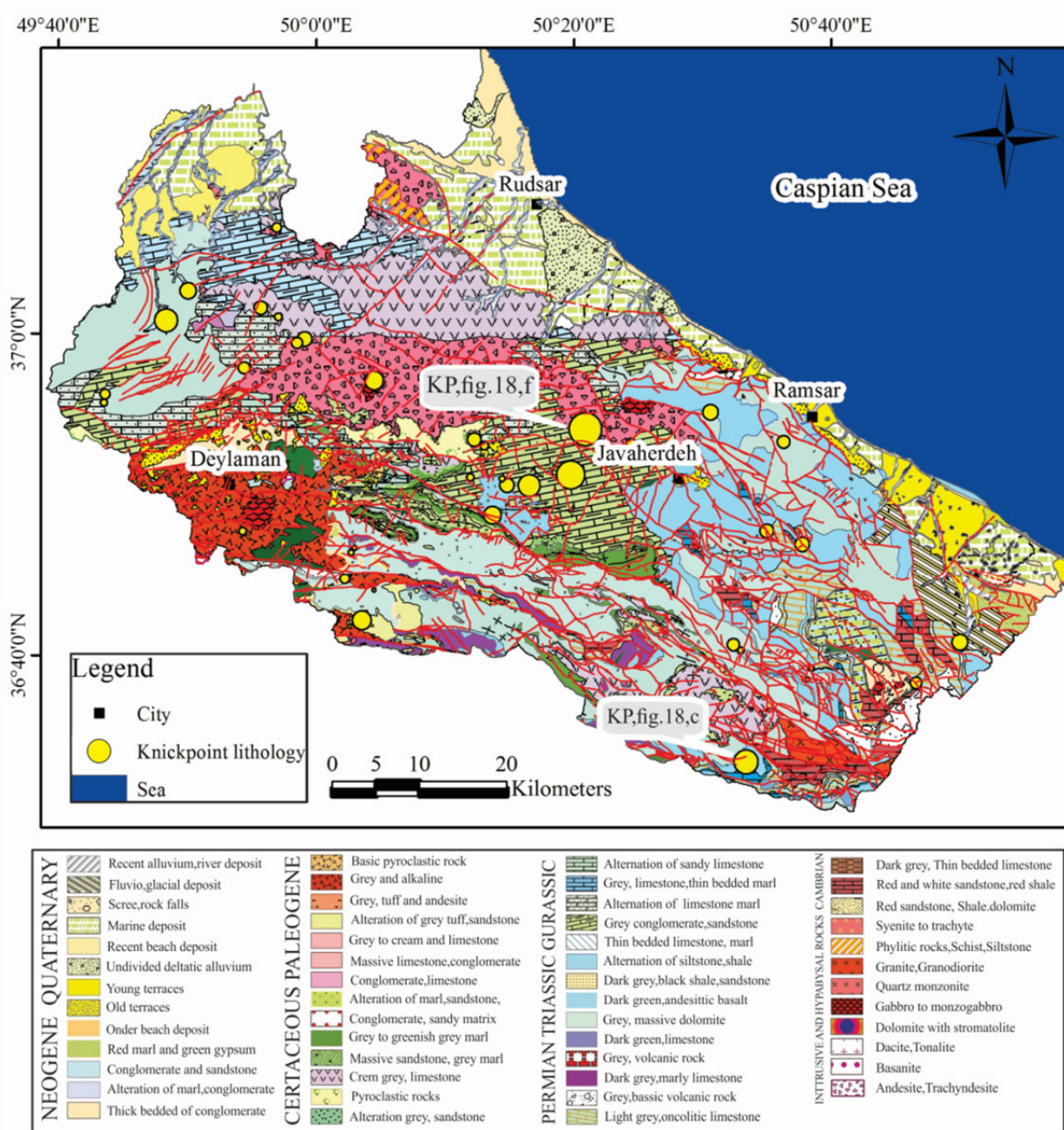


**Figure 2** Geological map of with the pattern of extractive 45 knickpoints on the different lithological units in the study area.

to local changes resulting from tectonic activities due to uplift or subsidence (Bull and Mcfadden 1977). The streams and sub-basins of the area were extracted from a filled G-ASTER 30-meter digital elevation model in the Arc Hydro plugin in Arc GIS 10.1 software. Then, necessary corrections were made utilizing topographic maps and satellite imagery, followed by determining active tectonic using morphometric indices. The six morphometric indices for this evaluation (i.e., stream length-gradient index (SL), hierarchical anomaly index

( $\Delta a$ ), Bifurcation index ( $R$ ), hypsometric curve and hypsometric integral ( $Hi$ ), relative relief index ( $Bh$ ), and basin shape index ( $Bs$ ) were measured in 38 sub-basins in the studied area. Eventually, the studied area was zoned into four tectonic classes of activity (i.e., extremely high, high, medium, and low) after measuring relative tectonic activity. The normalized steepness index ( $K_{sn}$ ), concavity ( $\theta$ ) in sub-basins, and knickpoint extraction were determined using a longitudinal profile, and geomathematics and geostatic methods,

respectively. Finally, the fieldwork was compared with the classes of active tectonic indices and the IAT index in order to analyze the results. Furthermore, active Quaternary faults were evaluated to demonstrate the evidence of tectonic deformations on the rivers, followed by measuring the direction of 34 Plio-Quaternary joints occurring in different sites of the Soheil fault and 44 Plio-Quaternary joints of the Deylaman fault. Additionally, the rose diagram of Quaternary fractures of the Deylaman and Soheil zone was constructed based on structural studies and field evidence.

### 2.1 Stream length-gradient index

Stream channels may be influenced by tectonic and lithologic changes, leading to anomalies in their longitudinal profile and thus the stream length-gradient index. Such disturbances typically imply the contrasts of erodibility between various lithological units and active tectonics including faulting (Seeber and Gornitz 1983; Merritts et al. 1994; Burbank and Anderson 2001; Bishop et al. 2005; Larue 2008). The stream length-gradient index (SL) is calculated for a specific pathway drainage network based on Eq. (1) (Hack 1957, 1973, 1982):

$$SL = (\Delta H / \Delta Lr) Lsc \quad (1)$$

where SL is the Stream length-gradient index,  $\Delta H$  is the topographic elevation height changes and  $\Delta Lr$  is the length of a reach,  $(\Delta H / \Delta Lr)$  is the slope of the channel or the gradient between the two contour lines and  $Lsc$  denotes the length of the channel from the source of the river to the midpoint of the two lines of topography for each sub-basin (Burbank and Anderson 2001).

### 2.2 Hierarchical anomaly index

The hypsometric integral ( $Hi$ ) describes the relative distribution of the elevation in a given area of a landscape, especially a drainage basin. Further, the index is defined as the relative area below the hypsometric curve and it is an important indicator of topographic maturity (Strahler 1952). Furthermore, the hierarchical progressive of a basin is divided into stream segments in the drainage system (Horton 1945). It should be noted that the number of stream junctions increases by

increasing the stream order and a first-order stream produces a second-order stream ( $1 \rightarrow 2$ ), then the second-order stream provides a third-order ( $2 \rightarrow 3$ ), and so forth. For instance, a basin with the highest stream order of 5 has 10 stream junctions ( $1 \rightarrow 2, 1 \rightarrow 3, 1 \rightarrow 4, 1 \rightarrow 5, 2 \rightarrow 3, 2 \rightarrow 4, 2 \rightarrow 5, 3 \rightarrow 4, 3 \rightarrow 5$ , and  $4 \rightarrow 5$  junctions) (Strahler 1957). Some stream junctions have hierarchical anomalies when lower stream orders flow in higher orders ( $1 \rightarrow 3, 1 \rightarrow 5, 2 \rightarrow 4, 2 \rightarrow 5$ , etc.) (Ciccacci et al. 1987).

The hierarchical anomalies index is calculated based on the number of hierarchical anomalies (Ciccacci et al. 1987), expressed by:

$$Hai \rightarrow j = 2^{(j-2)} - 2^{(i-2)} \quad (2)$$

where  $i$  is the primary stream,  $j$  is end stream and  $Hai \rightarrow j$  the number of hierarchical anomalies of each stream. The number of hierarchical anomalies has been calculated in Eq. (3):

$$Ha_t = \sum (Ha_i \rightarrow j \times Ns_i \rightarrow j) \quad (3)$$

where  $(Ns_i \rightarrow j)$  is the total number of streams entering the high-level streams.

The index  $\Delta a$  is expressed by the following relationship (Guarnieri and Pirrotta 2008).

$$\Delta a = Ha_t / N_1 \quad (4)$$

where  $Ha_t$  is the number of the hierarchical anomaly and  $N_1$  is the number of first-order segments of the streams.

### 2.3 Bifurcation index

The Bifurcation index acts as a measure of the degree of branching and dissection experienced by the drainage basin during its evolution (Ciccacci et al. 1987; Guarnieri and Pirrotta 2008). This index relies on hierarchical anomalies and provides useful information about the type of the erosion process and the degree of the evolution of drainage basins (Guarnieri and Pirrotta 2008). The Bifurcation index has been calculated by the relation (5) (Baroni et al. 2005):

$$R = R_b - R_{db} \quad (5)$$

where  $R_b$  is the bifurcation ratio and  $R_{db}$  is the direct bifurcation. The bifurcation ratio of each stream category obtained from Eq. 6, divides the total number of streams of that order by the total number of upper-order streams (Horton 1945; Strahler 1952).

$$R_{b(u-u+1)} = N_u / N_{u+1} \quad (6)$$

where  $N_u$  is the number of streams of one order and  $N_{u+1}$  is the number of segments of all higher-order. The index  $R_{db}$  is calculated by Eq. (7)

$$R_{db} = N_{du}/N_{u+1} \quad (7)$$

where  $N_{du}$  is the number of specially order that run to higher-order and  $N_{u+1}$  is the number of streams of a higher order.

## 2.4 Drainage basin shape

The horizontal projection of a basin described by the Drainage basin shape index or the elongation ratio (Cannon 1976; Ramírez-Herrera 1998), The  $B_s$  can be determined by Eq.(8) as follows:

$$B_s = Bl/Bw \quad (8)$$

where  $Bl$  is the length of the basin measured from its mouth to the most distant drainage divide and  $Bw$  denotes the width of a basin measured at its widest point.

## 2.5 Hypsometric integral and curve index

The hypsometric integral is a stage measure, and geomorphic development can be evaluated with the hypsometric integral (Strahler 1952). In addition, the  $H_i$  index is defined as the area below the hypsometric curve, and thus expresses the volume of a non-eroded basin (Pike and Wilson 1971). Further, the hypsometric integral and the curve index of the basin are determined by plotting the total relative height versus the total area (Keller and Pinter 2002).

$$HI = (\text{average elevation} - \text{min elevation}) / (\text{max elevation} - \text{min elevation}) \quad (9)$$

## 2.6 Relative relief

The Relative relief is defined as the ratio between the highest and lowest points of a basin and further height indicates higher uplift rates (Keller and Pinter 2002). This index is defined by Eq. (10):

$$Bh = H_{max} - H_{min} \quad (10)$$

## 2.7 Calculation of relative tectonic activity (IAT)

In the present study, six morphometric indices were calculated and relative tectonic activities were

ascertained accordingly. The mean value of the geomorphic indices ( $S/n$ ) of each basin was determined as well.  $S$  is the sum of numbers for different indices of a basin and  $n$  represents the number of indices used in each sub-basin. Additionally, the IAT index is classified into four classes: Class 1 ( $1.5 > S/n > 1$ ) and class 2 ( $2 \geq S/n > 1.5$ ), class 3 ( $2.5 \geq S/n > 2$ ), and class 4 ( $S/n > 2.5$ ) in terms of tectonic activity which correspond to intense, high, average, and low tectonic activities respectively. (El Hamdouni et al. 2008).

## 2.8 Normalized steepness index and Concavity index

Flint's empirical power-law defines the river profile in a steady-state (Flint 1974):

$$S = K_s A^{-\theta} \quad (11)$$

where  $S$ ,  $K_s$ ,  $A$ , and  $\theta$  indicate the slope, the steepness index, the drainage area, and stream concavity, respectively. In addition,  $K_s$  and  $\theta$  are directly computed by the regression analysis of the slope-area data (Whipple 2004; Wobus et al. 2006). Further, a steady-state landscape demonstrates that erosion, incision, and uplift rates are equal and stable over time (Whipple and Tucker 2002). Different empirical studies indicated a direct relationship between the value of the steepness index ( $K_{sn}$ ) and the bedrock erosion rate or rock uplift rate in the steady-state of river systems (e.g., Whipple and Tucker 1999; Kirby et al. 2003; Safran et al. 2005; Wobus et al. 2006):

$$K_s = (E/K)^{(1/n)} \quad (12)$$

where  $E$  denotes the uplift of the bedrock and  $K$  indicates the erosion coefficient which relies on the climatic and morphotectonics conditions of the area. Finally,  $n$  represents a positive exponent which is associated with the predominant erosion process of the area (Whipple and Tucker 1999; Kirby et al. 2003; Safran et al. 2005; Wobus et al. 2006). This quantitative relation demonstrates different uplift rates of the region in steady-state river profiles where vertical incision balances the rate of rock uplift (Kirby and Ouimet 2011). It is worth noting that a strong correlation exists between concavity ( $\theta$ ) and steepness indices ( $K_s$ ). The concavity range typically varies from 0.4 to 0.6 (Hack 1957; Flint 1974; Willgoose et al. 1990; Tarboton et al. 1991; Moglen and Bras 1995; Slingerland et al. 1998). In the present study,  $K_{sn}$



was normalized to a reference concavity  $\theta_{ref} = 0.45$ , (e.g., Kirby and Whipple 2001; Snyder et al. 2000; DiBiase et al. 2010) and these parameters were implemented to fit a steady-state stream power solution to individual river longitudinal profiles in Matlab (Topotoolbox). The best profile was obtained from the matching of the uplift rate ( $U = E$ ) or erosion ( $K$ ) and the predicted rate. Furthermore, normalized steepness and concavity indices were determined using the longitudinal profile of the river.

## 2.9 Knickpoints

A Knickpoint is a locally steep section of the longitudinal profile (Burbank and Anderson 2001; Schumm 2007). knickpoints were extracted along the rivers using two different methods (e.g., Burbank and Anderson 2001; Bull 2009a). More precisely, in the first method, the longitudinal profiles of the river were examined to detect knickpoints of the digital elevation model in Matlab software (GDEM) with 1 arcsec (~30 m) resolution (Kirby et al. 2007; Pederson and Tresler 2012). In the second method, the knickpoints are extracted using geological and geostatistical methods (Hayakawa and Oguchi 2006). Additionally,  $G_d$  was calculated through stream gradient along the rivers (Hayakawa and Oguchi 2006):

$$G_d = (E_1 - E_2) / d \quad (13)$$

where  $d$  is the horizontal length in meters, which was used to calculate the gradient, and  $E_1$  and  $E_2$  denote upstream and downstream elevations which are at a distance of  $d/2$  from the point of measurement derived from the digital elevation model. In addition, the gradient rate by increasing  $d$  is an index of relative steepness ( $R_d$ ) (Hayakawa and Oguchi 2006). The  $R_d$  curve illustrates fluctuations along the river, in which relatively fast parts correspond to large  $R_d$  values. The standard deviation of  $R_d$  was checked for each river and its average for all rivers was  $3.98 \times 10^{-6}$ . Further, river segments with a large amount of " $R_d$ " were determined as knickpoints. Eventually, the length and height of knickpoints were determined using the  $R_d$  curve, followed by measuring the boundary and extent of knickpoints according to upstream and downstream heights (Hayakawa and Oguchi 2006).

## 3 Results and Discussion

The Alborz range is part of the Alpine-Himalayas mountain belt, which lies in the south of the Caspian basin with a general W-E trend and a convexity to the south of the Alborz range (Berberian and King 1981; Allen et al. 2003). Different active faults are present along the Alborz range. This mountain range has an arcuate form which is part of the active deformation within the vast Eurasian-Arabian impact zone (Allen et al. 2003). Additionally, the seismology of the Alborz range represents active orogenic movements (Berberian and King 1981). The results of earthquake focal mechanisms demonstrated that the present general left-lateral shear is observed inside the central Alborz mountain range and associated with transtensional deformations (Jackson et al. 2002; Tatar et al. 2007; Berberian and Walker 2010). The observations represent that horizontal movements along strike-slip faults in the central and western Alborz have reversed the vertical component of the thrusting faults in the central part of the range. This is an example of extensional phenomena occurring within a compression-dominated region (Ritz et al. 2006). The study area comprises several tectonic elements which are active in Quaternary. Deylaman and Soheil faults tilted the Neogene, Quaternary sediments on a large scale. In addition, the existence of faults in tilted Quaternary sediments, deep fault valleys, and high bedrock and gorges evidence active structures supported by morphometric indices. Morphometric indices suggest that the main faults such as Soheil, Deylaman, Kashachal, Nusha, Samamous and Chalmehrud control the morphology of fluvial basins in the region. We confirmed the locations of the selected knickpoints and verified whether they were related to changes in lithology or to fault presence. We also present our results and analyses of the selected indices (i.e., longitudinal stream profiles, knickpoints, SL and  $K_{sn}$ ), which actually reflect of tectonic uplift in the study area.

### 3.1 Fieldwork

#### 3.1.1 Deylaman Fault

The Deylaman fault with an E-W trend has a steep dip to the north and a direction for the thrusting toward the south. Furthermore, the dip of the Deylaman fault in Kashkuh Mountain is nearly  $60^\circ$  to the north and its slickensides have a rake of about 78 degrees from the west with a dextral strike-slip component. Additionally, the difference between the thickness of Mesozoic and Cenozoic rock units on both sides of the Deylaman fault indicates that this fault has been active during the Jurassic, Cretaceous, Paleogene, and Neogene periods (Hakimi Asiabar and Bagheriyan 2018). In addition, this fault was active during the Mesozoic period as a normal fault and activated as a reverse fault during the Cenozoic period, representing an inversion in the tectonic style movement of deformation in the Alborz range (Figure 3). Several “thrusts” of the belt demonstrate a normal separation and interpret the assemblage as an asymmetrical, south-vergent, and transpressional positive flower structure (Axen et al. 2001). Further, the Alborz is a sinistral transpressional belt, where the slip is partitioned between sinistral strike-slip and thrust faults related to the inversion of pre-existent extensional normal faults (Jackson et al. 2002; Allen et al. 2003).

In the current study, field observation presents some evidence of Neogene-Quaternary inversions along the pre-existent normal faults of Central Alborz and structural evidence along Deylaman and Soheil faults. Neogene and Quaternary sediments are tilted by the Deylaman fault on a large scale (Figures 4, 5), and the average trend of the Deylaman fault is N38E (Hakimi Asiabar and Bagheriyan 2018). The rose diagram of the 44 Plio-Quaternary joints of the Deylaman zone was made based on field studies, where the average trend is N30E (Figure 5d) which is parallel to the Deylaman fault trend. These results with active landforms (Figure 6a, c) imply that the Deylaman fault zone has been active during the Quaternary and represents the geomorphic evidence of its activity in the future.

### 3.1.2 Soheil Fault

Furthermore, the Soheil fault has a northwest/southeast strike with a dip direction toward the northeast, causing uplift and displacement in units in addition to cutting the folds in this region during the Upper Cretaceous. The axis of the folds is



**Figure 3** A view of the Deylaman zone and thrusting of shale and sandstone of Shamshak on Cretaceous argillic limestone Deylaman village, the direction of the view is to the southeast.

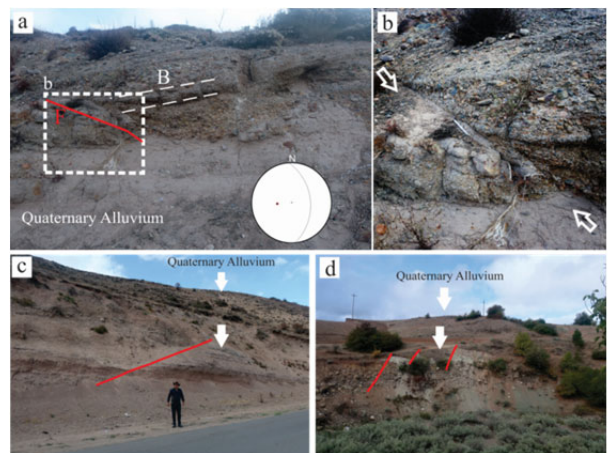


**Figure 4** Deformation of Neogene and Quaternary alluvial deposits along the Deylaman fault: (a,b) fractured Neogene conglomerate with  $175^\circ$  NE due to the Deylaman fault zone activity near Arashki village, west view, Stereonet showing the Quaternary fault, Fracture is marked by arrows. (c, d) Quaternary faulting and fracturing along the Deylaman fault zone activity near Deylaman village, the arrows indicate Quaternary Alluvium, West and Southwest view.

overturned along the fault, and the dip of the fault is about  $52^\circ$ - $55^\circ$  to the north with a rake angle of about  $75^\circ$  (Figure 7a,b) Additionally, the Soheil fault has been active during the Jurassic, Cretaceous, Paleogene, and Neogene periods (Hakimi Asiabar and Bagheriyan 2018). The mid-Jurassic rock units are thrust over the lower Cretaceous rock units (Baharfirouzi et al. 2005) and various Quaternary joints are observed in different parts along the Soheil fault zone in the study area (Figure 8).



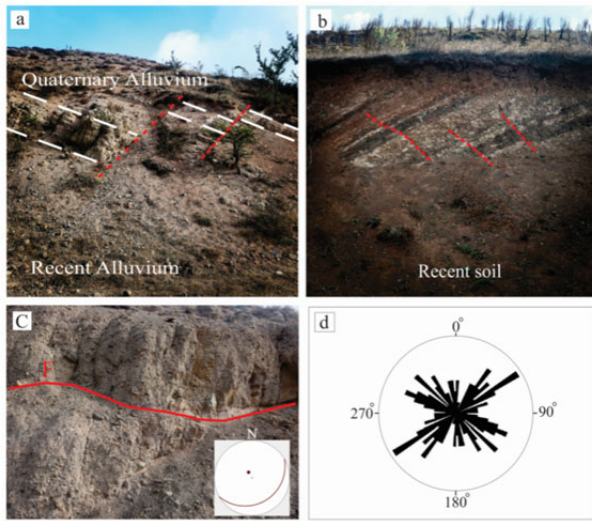


**Figure 5** Quaternary faulting, fracturing and young deformed Quaternary alluvial deposits along the Deylaman fault zone. Fractures are marked by arrows: (a) Faulting and tilting of Quaternary units along the Deylaman fault zone in Gohak village East view. (b) Quaternary fracturing and tilting of the layers in the Arashki village North view. (c) Fracture affecting the Neogene conglomerate with  $60^{\circ}/20^{\circ}$  NE at Asaiabar village, North view. (d) Rose diagram of the cumulative fracture strike data in the Quaternary deposits of the Deylaman fault zone.



**Figure 6** Morphotectonic landforms in the study area: (a) A deep gorge cutting created near Deylaman, South view. (b) A gorge of the soheil fault zone in the Upper Cretaceous in the Kakrud village, northwest view. (c) A view of the V-shaped valleys in the north of the Deylaman fault in Arashki village. (d) V-shaped valley in the north of the Soheil fault in Kakrud village.

The direction of 34 Plio-Quaternary joints occurring in different sites of the Soheil zone was measured in the present study. The average trend of the Soheil fault is as N55E (Hakimi Asiabar and

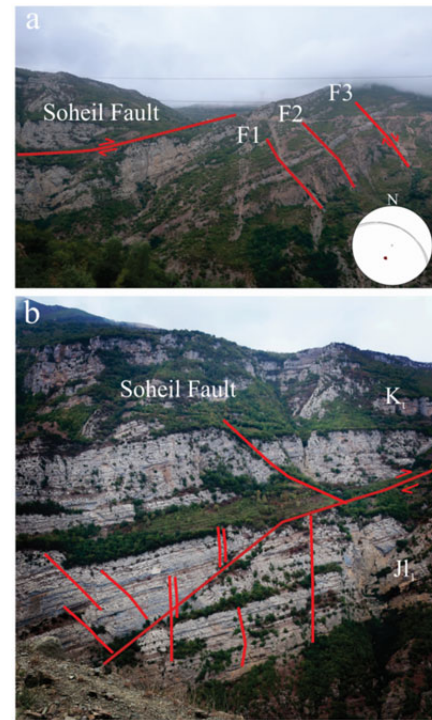


**Figure 7** Field photographs: (a) The thrusting of Tizkouh Formation on Lar Formation to the southwest by Soheil Fault and dip of fault to the northeast, West of Kakrud village, with a view to the south, stereo plot showing the faults F1, F2, F3 data. (b) Syntectonic normal faults in Lar formation in the upper Jurassic, south view.

Bagheriyan 2018). In addition, the rose diagram of Plio-Quaternary joints was constructed according to field investigations, and two joint sets were observed around the Soheil fault zone. The joint set with the N-E trend (Figure 8b, d, e) is more abundant compared to the N-W trend (Figure 8a). Accordingly, the direction of their averages is N60E (Figure 8c), which is parallel to the direction of the Soheil fault and is attributed to the movements of this fault based on structural studies and field evidence (Figure 6 b,d). Further, pliocene deposits atop Quaternary sediments and Quaternary joints indicate movements along with the Soheil fault.

### 3.2 Morphometric indices

The bifurcation index relies on hierarchical anomalies and provides useful information about the type of erosion processes (Guarnieri and Pirrotta 2008). More precisely, the hierarchical anomaly and bifurcation values of the drainage network have frequently been used as proxies for tectonic activity and are highly sensitive to the

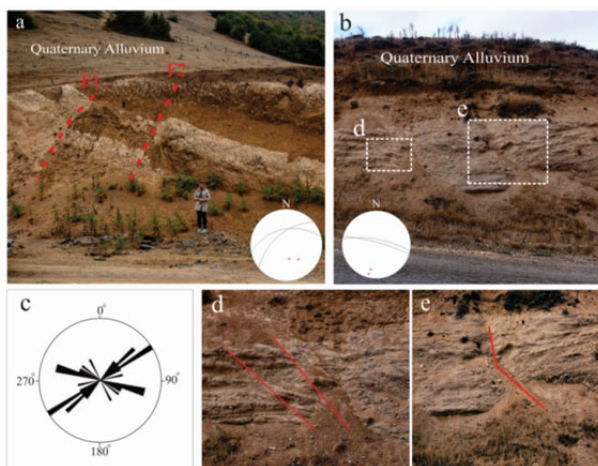


**Figure 8** Quaternary faulting and fracturing along the Soheil fault zone: (a) Quaternary faulting and fracturing along the Soheil fault,  $F1:50^{\circ}/36^{\circ}NW$  and  $F2:78^{\circ}/48^{\circ}NW$  and displacement of Quaternary deposits as well as tilting of layers near Kuhpas Village, northwest view and Stereo plot showing the faults F1, F2 data. (b) The Fracturing of Quaternary deposits in Hosnimahalleh Village, Northwest view, Stereo plot showing the fault planes. (c) Rose diagram of the cumulative fracture strike data in the Quaternary deposits of the Soheil fault zone. (d, e) Quaternary faults:  $100^{\circ}/75^{\circ}NE$  and  $110^{\circ}/80^{\circ}NE$ .

effects of tectonic activity on the geomorphic evolution (Ciccacci et al. 1987; Guarnieri and Pirrotta 2008). The bifurcation ratio value was higher than 1.5 for sub-basin 5 whereas the bifurcation ratio values were lower than 0.2 for sub-basins 20, 31, and 32. Figure 8 displays the number of the streams of Poulrud River with low order 1, 2, or 3 joining to higher order 5 or 6 in sub-basins with higher  $H_a$  values. In sub-basins 6 (with value  $\Delta a = 1.6$ ), 7 (3.71), and 8 (3) with higher  $H_a$  values, the number of the 2nd and 3rd order streams joins the 6th order streams. Further, the number of 3rd and 1st order streams joins the 5th and 3rd order streams in sub-basins 17 (1.92) and 18 (1.1), respectively. The rate of tectonic activity can be related to active faults which tectonically active at the intersection of the Polrud River due to active faults of Soheil, Deylaman, Zarrinrajeh, Samamous, and Chalmehrud (Figure 9).

Furthermore, the shape index of the basin, relatively young drainage basins in active tectonic areas, tends to be elongated in shape, normal to the topographic slope of a mountain. Conversely, it tends to be evolved to a more circular shape by continued evolution or less active tectonic processes (Bull and McFadden 1977). Additionally,

high values of  $B_s$  are associated with elongated basins, which is generally associated with relatively higher tectonic activity. On the other hand, low values of  $B_s$  indicate a more circular-shaped basin, which is typically associated with low tectonic activity. In addition, rapidly uplifted mountain fronts generally produce elongated, steep basins and the widening of the basins occurs from the mountain front up when tectonic activity represents a decline or ceases (Ramirez-Herrera 1998). Further, basin shapes become progressively more circular with time after the cessation of mountain uplifts, and the elongated shape of the sub-basin experiences the most tectonic movement. It is noteworthy that the most elongated sub-basins are related to the western and eastern sub-basins of the region and one explanation for this issue may be the more resistant lithology and thus the presence of the Kashachal and Nusha faults of the eastern part, as well as the Khazar, Chalmerud and Lahijan faults, leading to the uplift of the associated basins. The values of the basin shape ( $B_s$ ) vary from 1.28 (basin 34) to 3.87 (basin 11). Furthermore, the length to mean width ratio of the

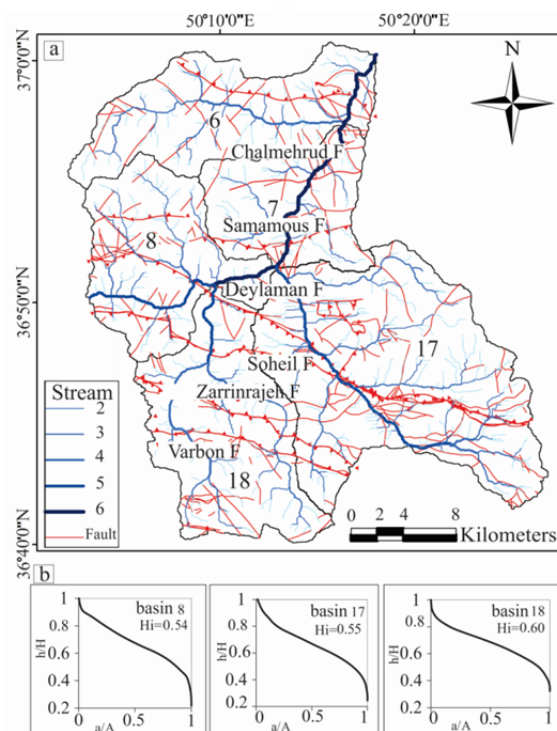


**Figure 9** (a) Anomaly map of the Hierarchical anomalies ( $\Delta a$ ) of the Polrud river, the number of 2, 3, 4, 5, and 6 in the figure are the number of order stream. (b) Hypsometry curves of three subbasins.

sub-basins ( $B_l/B_{mw}$ ) is lower than 1.5 in basins 34 and 36, representing their relatively circular shape. Additionally, the high values of  $B_l/B_{mw}$  ratio  $>3$  in sub-basins 1, 2, 3, 5, 6, 11, and 35 indicate elongated basins and higher length compared to the mean width of the mentioned basins. In addition, the  $B_l/B_{mw}$  ratio in other sub-basins ranges from 1.5 to 2.5, implying less elongated shapes. The obtained results demonstrate that  $\Delta a$  is correlated with the  $B_s$  index, and elongated and tilted sub-basins have higher values of  $\Delta a$  and  $R$  indices (Figure 10a, b, d). For example, the values of  $\Delta a$ ,  $R$ , and  $B_s$  are higher for basins 6, 11, and 35. Further data are provided in Table 1. In narrower

sub-basins, the  $\Delta a$  increases due to the joining of lower to higher order streams. Based on the results, elongated structural sub-basins located between the main faults had higher rates of  $\Delta a$  compared to nearly circular shape/erosional basins. Considering that the elongation (shape) and tilting of basins are controlled by variations in the rates of the hierarchical anomaly of the drainage systems of studied basins is controlled by tectonic activities. The extremely low values of the bifurcation ratio and  $\Delta a$  in the only available northern basins can be attributed to the differences in basins lithology (Figure 10a). The hypsometric integral varies from 0 to 1, and the values of near-zero at higher-eroded

**Table 1** The values of the morphometric indices and the relative tectonic activity classes (IAT).

Basin no.	Area <sup>a</sup> (Km <sup>2</sup> )	SL <sup>b</sup> Class	$\Delta L^c$ Class	$R^d$ Class	Hi <sup>e</sup> Class	Bh <sup>f</sup> Class	Bs <sup>g</sup> Class	Iat <sup>h</sup> Value	Iat Class
1	276.56	327	1.01	1.05	0.14	1443	3.2	1.5	1
2	244.76	711	0.76	1.07	0.30	2144	3.35	1.66	2
3	295.64	353	1.72	0.92	0.18	1644	3.67	1.66	2
4	173.45	1768	0.96	1.26	0.4	2419	2.35	1.66	2
5	233.02	255	0.49	1.52	0.14	1469	1.81	2.33	3
6	145.92	1089	1.6	1.18	0.45	2339	3.12	1	1
7	102.76	810	3.71	0.60	0.35	2734	2.05	1.33	1
8	130.92	1015	3	1.25	0.54	1921	2.06	1.16	1
9	317.75	289.4	0.93	0.93	0.44	1486	2.04	1.16	1
10	30.07	68	0.25	0.75	0.38	82	1.46	2.66	4
11	51.33	340	3.79	0.88	0.17	1258	3.87	1.83	2
12	31.29	3	0.38	0.87	0.17	933	1.45	2.66	4
13	28.52	257	0.18	0.25	0.17	877	1.45	3	4
14	100.88	1226	0.46	0.72	0.38	3508	2.12	1.5	1
15	11.16	278	0.18	0.33	0.11	759	1.44	3	4
16	130.29	1408	0.82	0.88	0.34	3715	3.1	1.16	1
17	285.70	1274	1.92	2	0.55	3206	2.05	1	1
18	165.69	982	1.1	1.21	0.60	2656	2.59	1	1
19	156.93	907	0.66	1.06	0.51	1989	2.15	1.33	1
20	11.46	31	0	0	0.40	85	1.5	2.83	4
21	36.01	655	0.13	0.25	0.23	1742	1.58	2.5	3
22	81.01	1069	0.2	0.58	0.34	2551	1.49	2	2
23	159.72	1138	0.87	0.94	0.36	3600	1.67	1.5	3
24	35.05	545	0.11	0.25	0.21	1299	1.52	2.66	4
25	80.22	736	0.35	0.39	0.22	2179	1.5	2.5	3
26	167.04	1340	1.09	0.74	0.55	3092	2.08	1.16	1
27	110.33	829	2.34	0.44	0.37	2808	2.06	1.33	1
28	144.74	1316	0.9	1.16	0.52	2944	2.15	1	1
29	283.09	937	0.55	0.92	0.47	2678	2.2	1.16	1
30	226.18	1242	0.99	0.79	0.28	3570	2.37	1.5	2
31	19.78	289	0	0	0.19	1179	1.5	3	4
32	23.81	39	0	0	0.32	117	1.52	2.83	4
33	26.62	33	0.2	0.67	0.17	352	1.5	2.83	4
34	36.96	62	0.22	0.3	0.10	647	1.28	3	4
35	372.84	1851	1.67	0.93	0.45	4063	3.17	1	1
36	32.47	439	0.11	0.2	0.33	114	1.33	2.66	4
37	91.47	916	0.76	0.39	0.32	2564	1.87	1.83	2
38	134.43	829	0.97	1.05	0.39	2080	2.3	1.33	1

**Note:** a, Total area of the basin; b, Stream-gradient index; c, Hierarchical anomaly index; d, Bifurcation index; e, Hypsometric integral index; f, Relative relief index; g, Drainage basin shape index; h, Relative tectonic activity index.



areas and values close to one represent areas with minimal erosions and uplifts (Pedrera et al. 2009). The results of hypsometric integral values are listed in Table 1. As shown, the minimum value is 0.10 for sub-basin 34 while the maximum value is 0.6 for sub-basin 18 with a young convex topographic curve and high-rise elevations with deep valleys in the middle of the range influenced by the activity of Kashachal and Nusha faults (Figure 10c). Furthermore, the high hypsometric index value in sub-basins 8-17-18 is  $H_i > 0.5$  and displays ruggedness and youthfulness in accordance with Soheil and Zarrinrajeh faults (Figure 10c). Based on the observations, northern sub-basins indicate the low value of this index (smaller than 0.3) with the concave curve of the coastal drainage aging stage (Figure 10c).

It should be noted that basin relief plays an important role in the development of drainage, permeability, the surface of landforms, the

characteristics of the terrain erosion, and water movements on the surface and underground (Schumm 1956). The most relief and the highest rate of tectonic activity based on this indicator is observed in sub-basin 35 (with a value of 4063), which relies on the activity of Nusha and Kashachal faults. The values of the Bh index are provided in Table 1. Based on the Bh values of sub-basins ranging from 82 (basin 10) to 4063 (basin 35). The highest reliefs in the southeast basins had an elevation of over 2000, indicating the elevation and youthfulness compared to the average drainage basin (Figure 11c). Additionally, stream length-gradient (SL) values demonstrate longitudinal profile abnormalities, and these abnormalities represent erodibility contrasts between different lithological units and active tectonics including faulting (e.g., Seeber and Gornitz 1983; Burbank and Anderson 2001; Harkins et al. 2005; Larue 2008). In the present study, the SL map was

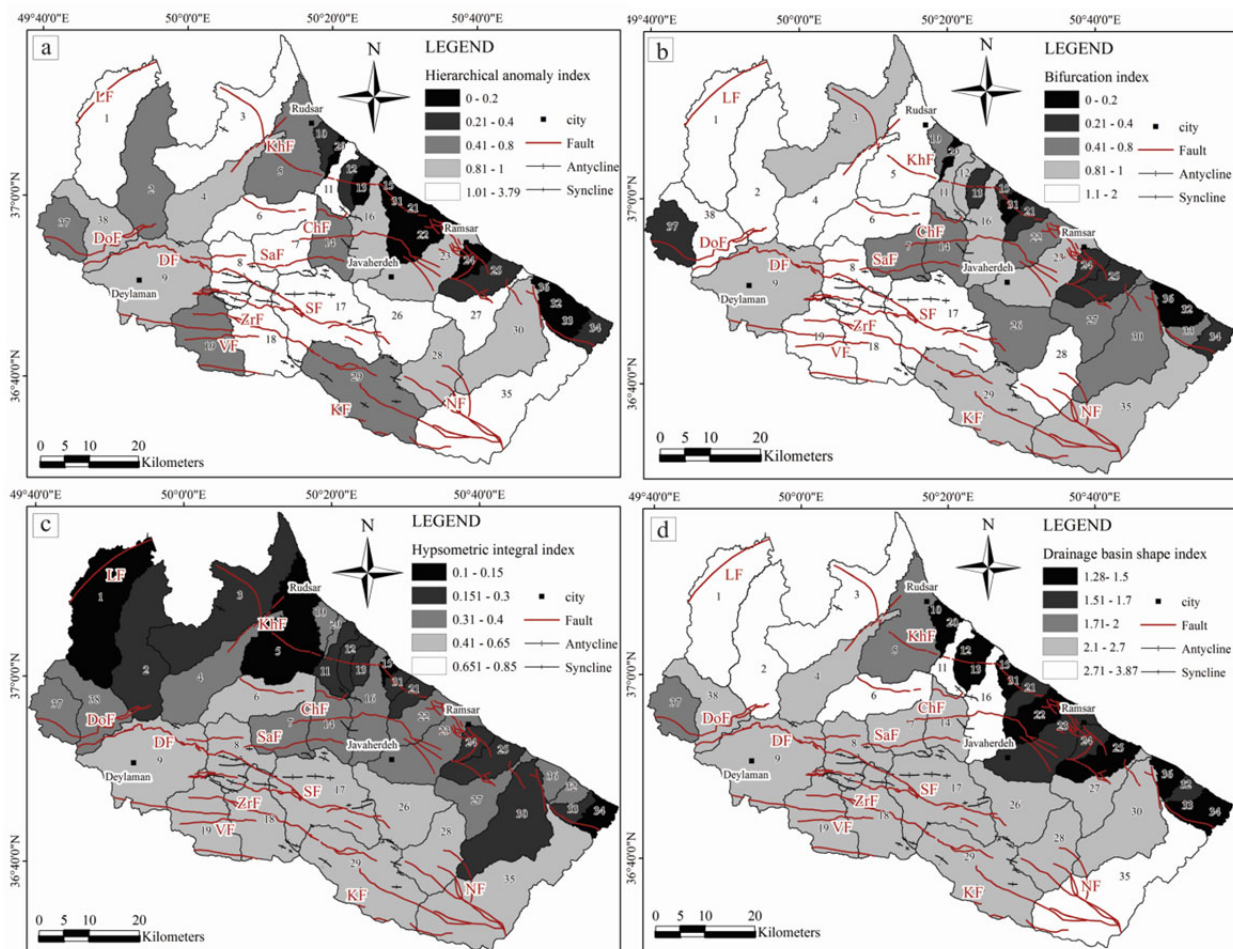


**Figure 10** The indices maps of the study area: (a) Distribution of  $\Delta a$  classes (b) Distribution of  $R$  classes (c) Distribution of  $H_i$  classes (d) Distribution of  $B_s$  classes.

designed for tracking SL anomalies along the main rivers of each sub-basin. Based on the results, low SL values indicate less active tectonic areas and areas where rivers cross less resistant bedrocks, indicating stable conditions. On the other hand, anomalously high SL values suggest more tectonically active regions, highly erosion-resistant bedrocks, or migratory knickpoints, are defined as sudden changes in the longitudinal gradients of the river (Keller 1986; Keller and Pinter 1996; Whipple and Tucker 1999), and include forms such as steep rapids and waterfalls (Crosby and Whipple 2006). The highest SL index belongs to the intersections of faults and conjugate fractures which cut off the mainstream. In addition, the abnormal values in the SL index are related to sub-basin 35 with a mean value of SL (1852) influenced by the activity of Nusha and Kashachal faults and sub-basin 4 with the mean value of SL (1770) due to the Khazar fault activity. Contrarily,

the lowest SL value is three for the coastal sub-basin 12. In general, most coastal sub-basins associated with the Khazar fault display low SL index values. Further, abnormal values in the SL index are high in areas where the rock resistance is high or there is a broken slope along the river (where there is a waterfall) (Keller and Pinter 1996). Based on the results, high abnormal values in the SL index in the Polrud River and the formation of a waterfall in sub-basin 17 do not coincide with lithology boundaries. Therefore, SL anomalies related to slope changes are influenced by the structural activities of the Soheil fault (Figure 19a). Furthermore, the uplift caused by faults such as Soheil and Nusha in the middle and southern sub-basins represents high activities and high abnormal values of these sub-basins (Figure 10b). Based on the IAT class-map, the study area was divided into four classes including extremely active 66% (3207 km<sup>2</sup>) and active 24% (1174 km<sup>2</sup>) sections and

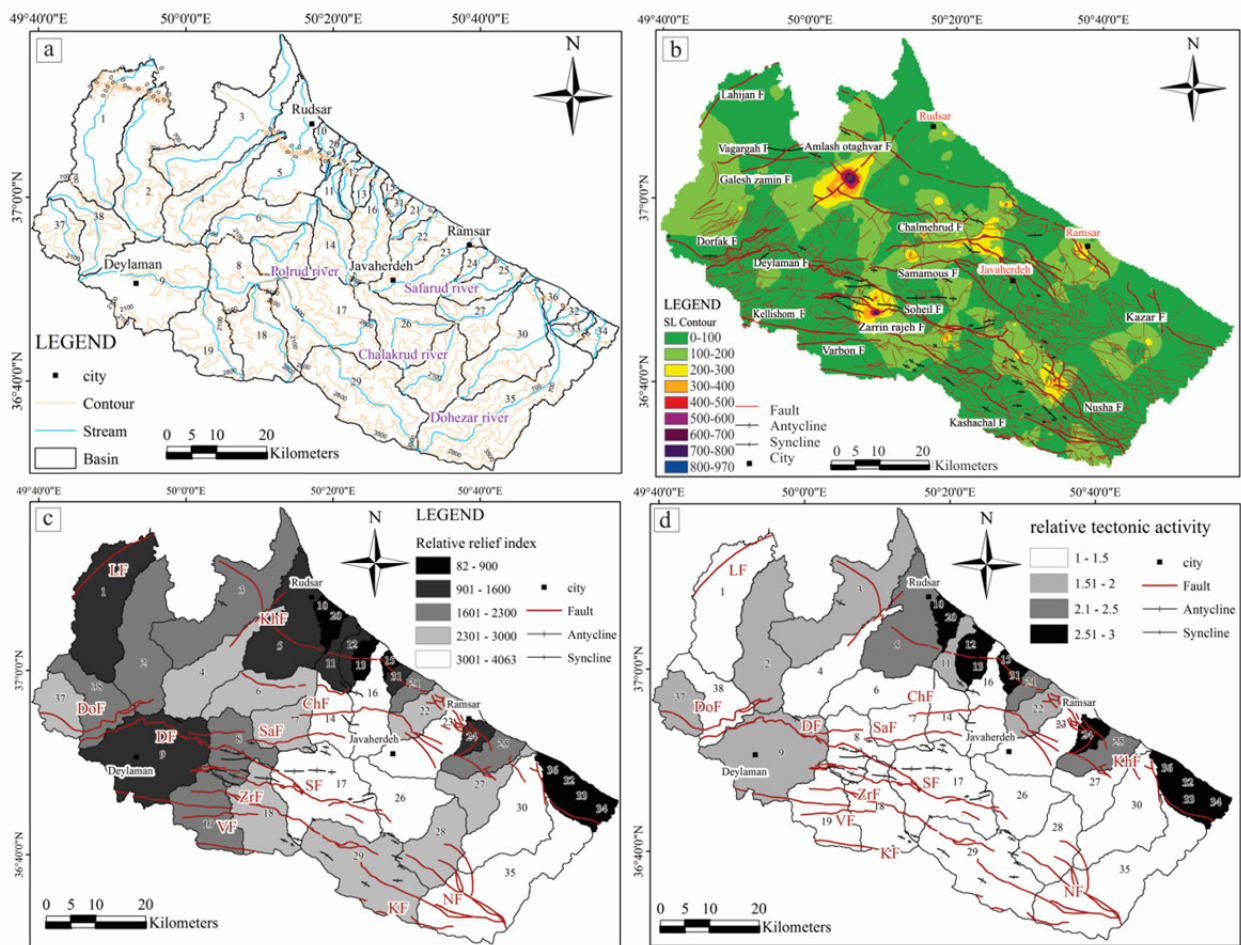


**Figure 11** (a) Map of the streams, Contour and 38 sub-basins of the region, (b) The Contour lines of SL index values in the study area, (c) Distribution of Bh classes, (d) Distribution of the relative tectonic activity (IAT).

average 7% (312 km<sup>2</sup>) and low 4% (214 km<sup>2</sup>) activities in the 1st and 2nd, as well as the third and fourth classes, respectively. [Table 1](#) presents the values of morphometric indices and the IAT index obtained for the basins of the study area. Additionally, the IAT map demonstrated that the main rivers such as Polrud, Dohezar, Safarud and Chalakrud of the region ranked in the first category of the relative tectonic index. Based on the zoning map of this assessment index, a high relative tectonic activity exists along the fault zones of Samamous, Nusha, Soheil, Deylaman, Kelishom, Zarrinrajeh, Kashachal, Dorfak, Varbon, and Chalmehrud and parts of the Khazar based on the index of active tectonics (IAT), which had a significant impact on the current topography and landform creation according to field evidence ([Table 1](#), [Figure 10d](#)).

The earthquakes of Rudsar on December 13, 1979, with (MW 5.0) and on December 23, 1979 (MW 5.1), also included southwest Tonekabon earthquakes on December 29, 1990 (MW 4.8) and December 29, 1990 (MW 4.3), earthquakes May 28, 2004, Baladeh-Kojour (MW 2/6), the 2005 Gorgan earthquake (MW 3/5), and the Gorgan earthquake of 1874 (MW 5/6), all of which is influenced by the activity of the Khazar fault and Active tectonics of Manjil-Rudbar fault zone ([Tatar et al. 2007](#); [Berberian and Walker 2010](#)) was studied due to the existence of several active faults and large-magnitude earthquakes documented in western Alborz. In addition, the earthquakes of the study area have magnitudes of Mw 5, all of which are influenced by the activity of the Khazar fault ([Berberian and Walker 2010](#)). Therefore, the Khazar fault is active at present based on these earthquakes and the role of the Khazar fault in increasing the SL anomaly in some parts of the fault, especially in Ramsar, along with increasing the gradient index in the basins of the Khazar fault ([Figure 11b](#)). The Kashachal fault (Jirandeh) represents class 1 active tectonics. The earthquake on August 15 (1485) in the AD of Mazandaran-Gilan is assumed to be due to activities on the Kashachal fault. Further, the earthquake on June 20 (1990) in Rudbar-Tarom with (MW 7.3) is due to the sinistral strike-slip mechanism with a break on the western part of the Kashachal fault ([Berberian and Walker 2010](#)). Active tectonics of Khazar, Samamous, Zarrinrajeh, Soheil, Deylaman,

Kashachal, Nusha, Dorfak, Chalmehrud, Lahijan, Kelishom, and Varbon faults, etc. whose movement caused destructive earthquakes in the area. Therefore, based on these earthquakes and the high value of IAT in this fault, the Kashachal fault is considered as one of the active faults which should be considered in seismic tectonic studies. Thus, the previous earthquakes of the faults of the region increase seismic risk evaluations based on the high relative tectonic activity and the historical earthquakes. Furthermore, they are responsible for the earthquake in the future.

Additionally, different values of the steepness index ( $K_{sn}$ ) along the river indicate a change in the inclination of the river due to the variability of the floor erosion of the channel floor or the uplift of the bedrock ([Kirby et al. 2003](#)). In addition, channels with high and low normalized steepness indices are categorized as high- and low-uplift areas, respectively ([Snyder et al. 2000](#); [Kirby and Whipple 2001](#); [Vanlaningham et al. 2006](#)).

Further, the concave profile represents a long-term equilibrium between erosion and uplift. Furthermore, the convex-concave longitudinal profile displays the predominance of the erosion for a long time and the low uplift rate and convex longitudinal profile represent the dominant uplift of the region ([Hovius 2000](#); [Kirby and Whipple 2001](#)). Additionally, low concavity and steepness indices demonstrate the young stage and the existence of active tectonics on morphological features. In addition, a high concavity index with a low slope indicates low tectonic activity and its aging stage ([Shahzad et al. 2009](#)). In the present study, normalized steepness values ( $K_{sn}$ ) were divided into four classes using quantiles. Classes 1 ( $100 \geq K_{sn}$ ) and 2 ( $50 \leq K_{sn} < 100$ ) represent high and average levels of tectonic activity, and Class 3 displays low tectonic activity in the region ([Table 2](#)). Further, the activity of the main faults of the area and the classification of the streams are illustrated by normalized steepness ( $K_{sn}$ ) and concavity indices ( $\theta$ ) ([Figure 12](#)). The presence of dip-slip faults at the basin level leads to a local increase in the steepness of the streams which are perpendicular to or oblique, and is considered as an effective factor in increasing the value of the normalized steepness index ( $K_{sn}$ ). Therefore, the degree and category of fault activity are characterized based on changes in this index.



**Table 2** Values and classes of Concavity index  $\theta$ (a) and Normalized steepness  $K_{sn}$  index (b).

Basin no.	Area (km <sup>2</sup> )	$\theta^a$	$K_{sn}^b$
1	276.56	0.4	107
2	244.76	0.71	127
3	295.64	0.74	132
4	173.45	1.1	162
5	233.02	0.43	187
6	145.92	0.5	195
7	102.76	0.23	144
8	130.92	0.35	87.5
9	317.75	0.59	112
10	30.07	0.53	3.92
11	51.33	0.35	106
12	31.29	1.1	40.1
13	28.52	0.19	73.5
14	100.88	0.6	305
15	11.16	0.51	62.7
16	130.29	0.85	302
17	285.7	0.42	245
18	165.69	0.2	160
19	156.93	0.2	218
20	11.46	0.4	4.76
21	36.01	0.21	136
22	81.01	0.42	286
23	159.72	0.21	274
24	35.05	0.93	104
25	80.22	0.35	147
26	167.04	0.45	271
27	110.33	0.54	160
28	144.74	0.47	380
29	283.09	0.15	202
30	226.18	0.26	286
31	19.78	0.34	111
32	23.81	0.48	7.88
33	26.62	0.34	6.61
34	36.96	0.53	46.9
35	372.84	0.46	273
36	32.47	0.12	9.78
37	91.47	0.27	150
38	134.43	1.1	270

**Note:** a, Concavity index; b, Normalized steepness Index.

Based on the results of the concavity index and the normalized steepness index in the sub-basins of the area, the maximum value related to the normalized steepness of the Porlud River of sub-basin 28 with a value of 380 and the index of 0.47 is close to the reference concavity and demonstrates enhanced uplifts. Furthermore, the average value of the normalized steepness index in coastal sub-basins, which are alluvial in the embayment of the Caspian Sea, is generally found to be low although this indicator increases in the area where the streams cut the Khazar fault, confirming the impact of the tectonic activity of the Khazar fault on the streams

(Figure 12a).

Some studies indicate that the Stream length-gradient index (SL) and the normalized channel steepness index ( $K_{sn}$ ) are also sensitive to rock resistance in other areas with high uplift rates (Whipple and Tucker 1999; Kirby et al. 2003; Duvall et al. 2004; Perez Pena et al. 2010). We determined the impact of lithology on the calculated indices by comparing the obtained results with lithological maps verified in the field. Therefore, the different values of  $K_{sn}$  and SL indeed reflect the effects of varying tectonic forcing processes and observed changes in elevation reflect differences in relative uplift within the study area. Variations in lithology can affect SL values when rivers flow across various rock units presenting different levels of resistance (Hack 1973). Hence, we implemented lithological units on the resulting SL values and locations of anomalously high SL values related to the boundaries between units of contrasting lithology (Figure 13). Therefore, the observed SL anomalies are related to active tectonic processes and lithological changes. An analysis of  $K_{sn}$  patterns imposed on the lithological map shows that the  $K_{sn}$  values are associated with differences in rock type. By comparing the  $K_{sn}$  values with geological maps, we found that the high  $K_{sn}$  values calculated for basins 1, 2, 3 and 29 are located lithological boundaries, and gently suggest the presence of relatively high uplift in these basins (Figure 13). Other high  $K_{sn}$  values observed do not seem to be correlated to changes in lithology. The highest levels of relative tectonic uplift confirmed by the high values of mean and maximum elevation SL, and  $K_{sn}$  in the center of the study area. Geomorphic indices values for the largest basin 35, which is located in the eastern part of the study area, also suggest high levels of relative uplift with high elevation in this area. The high SL index values were evaluated for the middle sections of rivers located in the central and eastern parts of the Alborz Mountain. A distribution of the normalized channel steepness index shows higher values of river segments in central and eastern parts of the study area and higher relative uplift. We found the results of this study suggest differences in relief and topographical features in the central Alborz Mountain as a consequence of differential tectonic uplift. Indeed, geomorphic indices (SL and  $K_{sn}$ ) calculated for basins in the northern part of the

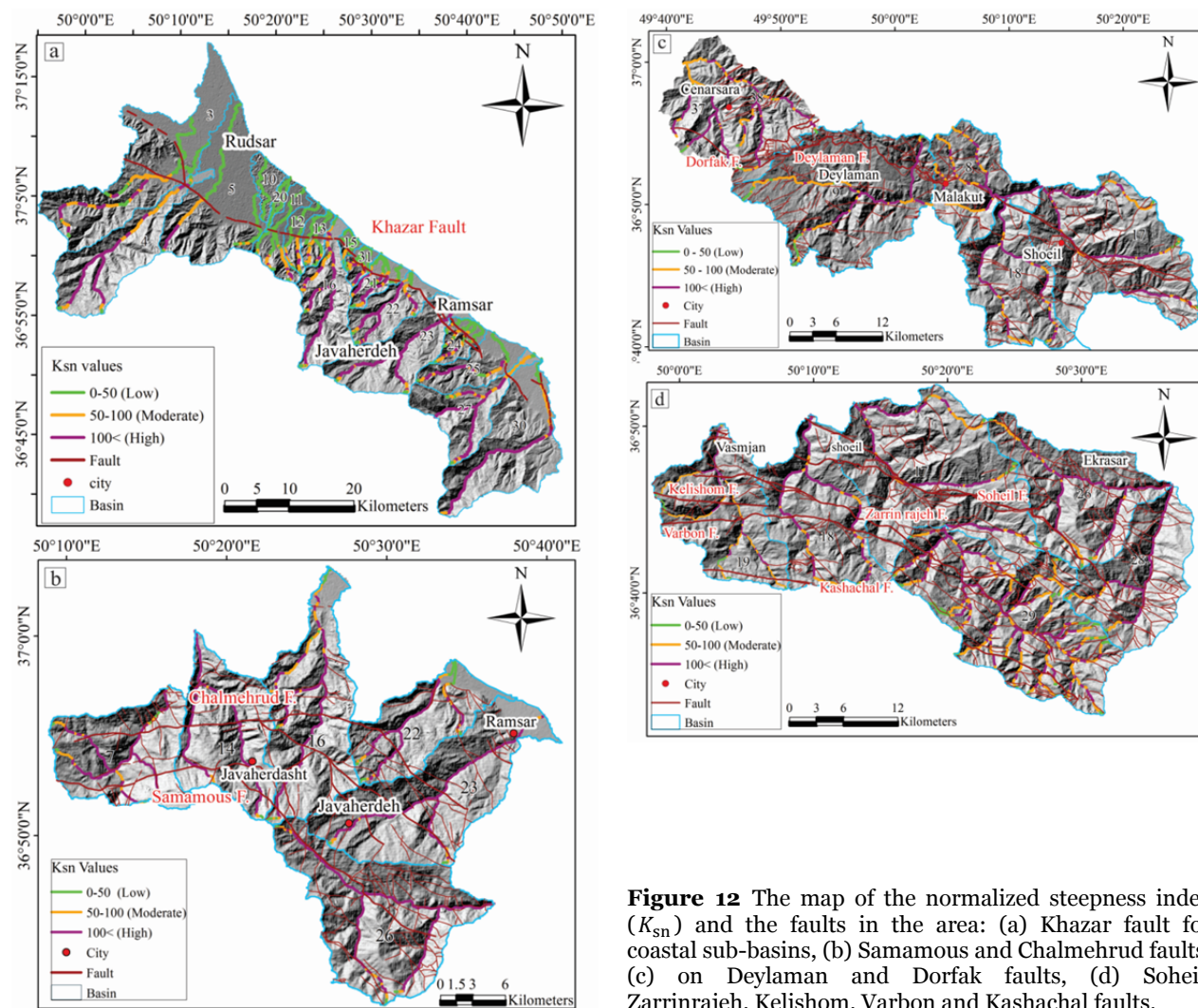


**Figure 12** The map of the normalized steepness index ( $K_{sn}$ ) and the faults in the area: (a) Khazar fault for coastal sub-basins, (b) Samamous and Chalmehrud faults, (c) on Deylaman and Dorfak faults, (d) Soheil, Zarrinrajeh, Kelishom, Varbon and Kashachal faults.

study area suggest relatively lower uplift levels and morphometric indices examined in this study suggest lower relative uplift patterns for these basins.

### 3.3 Knickpoint

Additionally, a knickpoint is a steep reach in a long fluvial profile which indicates the incision of regional bed incision (Gardner 1983). This steepening may be a response to an increase in shear stress or a decrease in shear strength or a reflection on the resistant lithology of the region (Hack 1957 1973; Bishop and Goldrick 2010). 150 major knickpoints were identified along the main rivers with more than 10-m in the study (Figure 14). Accordingly, field results imply that the lithology and structure of the bedrock are considered as the

significant factors of knickpoints (Figure 2). The lithological knickpoints also are easily recognizable in the field as waterfalls (Figure 2) (e.g., Miller 1991; Alexandrowicz 1994). Based on the findings, the distribution pattern of knickpoints with lithological units demonstrates no structural effect in the area. Our results indicate that structure is an important control affecting the Knickpoint.

The Polrud River, as the primary study channel, is regarded as an important stream located in the center of the study area. Further, Soheil, Zarrinrajeh and Kashachal faults, which represent dip directions toward the south, present high  $K_{sn}$  values thus the uplift of the hanging walls of these faults and the progressive increase of  $K_{sn}$  (Figure 12d). Therefore, a high normalized steepness value of more than 200 in the area can be observed where the Zarrinrajeh fault crosses the



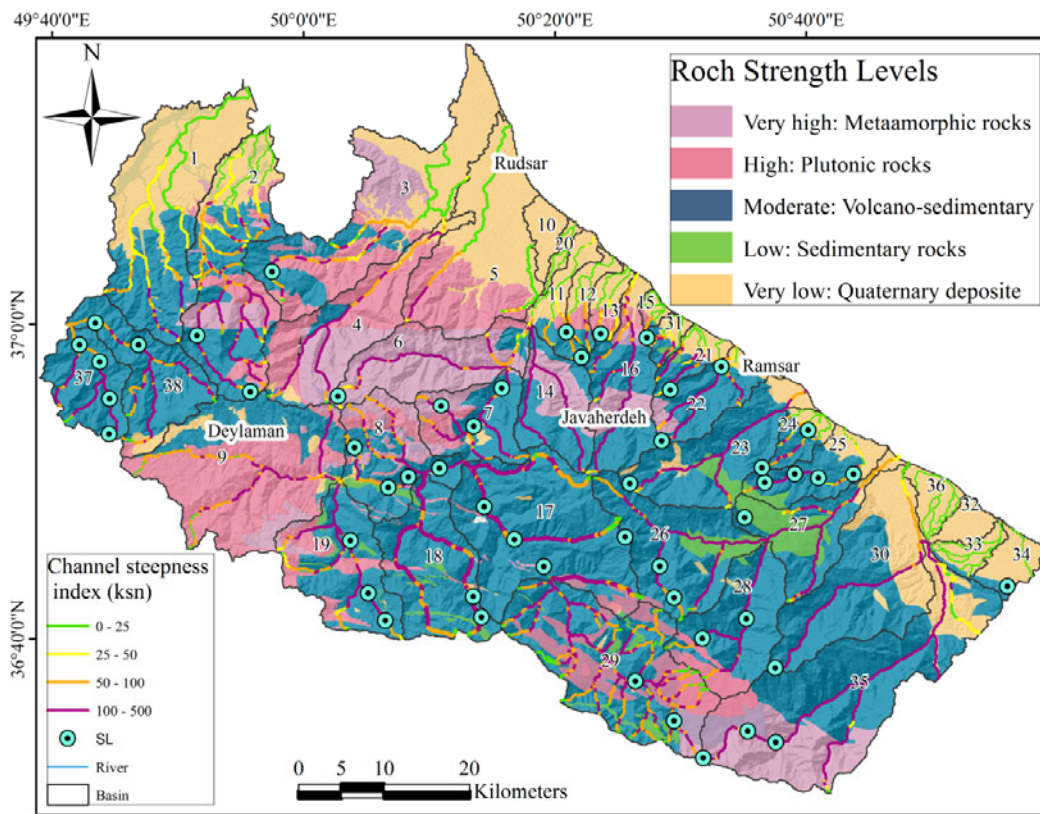


**Figure 13** Spatial distribution of SL anomalies and  $K_{sn}$  values for distinguished segments of the main rivers imposed on lithology in the Central Alborz Mountain.

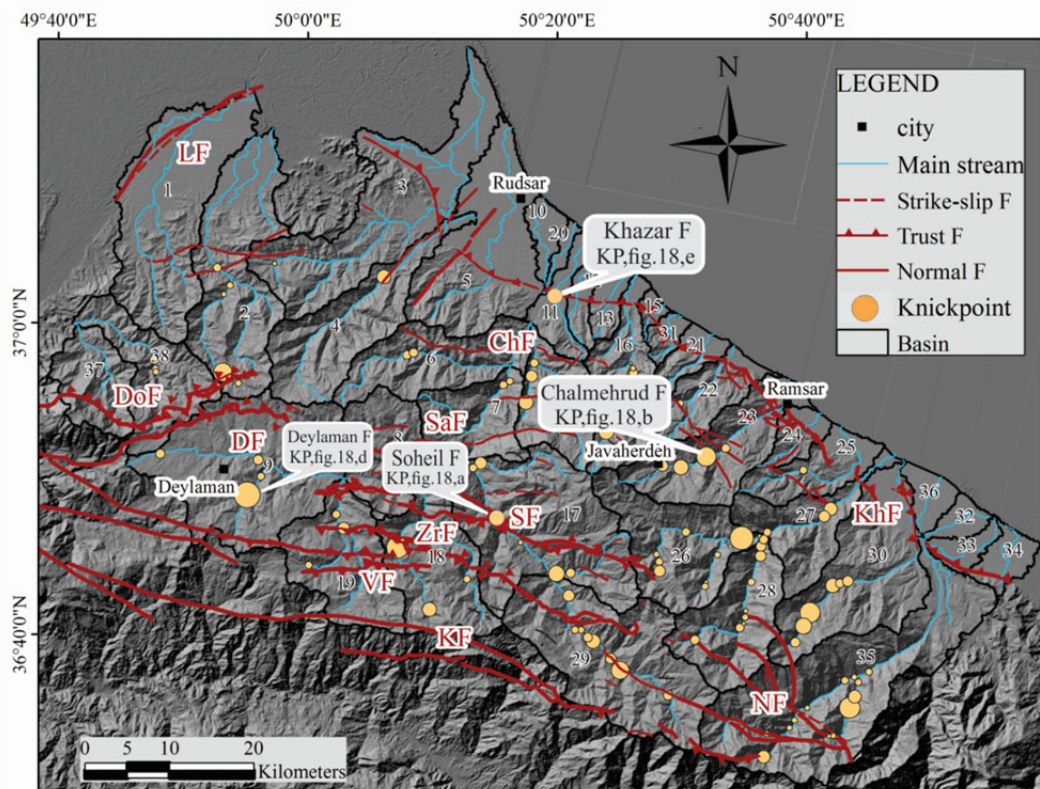


**Figure 14** Map of the pattern of distribution of extractive 105 tectonic Knickpoints (KP) in the study area.



river (Figure 15a). In the upstream part of the river profile, the amount of the concavity index is 0.2, which is due to the low erosion rate of river sediments. Furthermore, the Kashachal fault is a

sinistral strike-slip with a dip direction toward the southeast and displays a sinistral displacement of 200 meters (Berberian and Walker 2010). Additionally, the value of the concavity index is

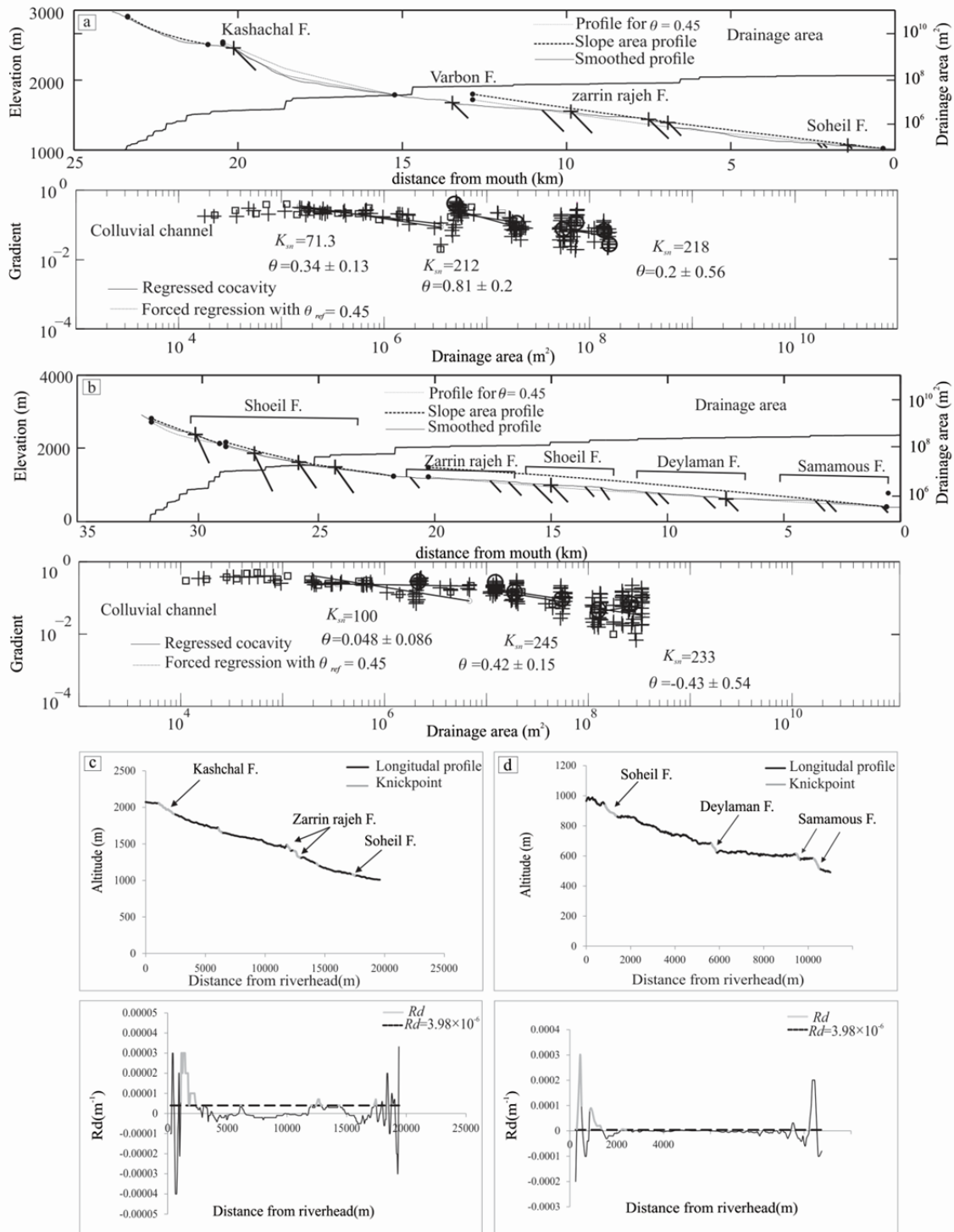


**Figure 15** (a,b) Longitudinal channel profiles and associated slope–area, log-log plots with best-fit regression lines defining concavity and gradient values for the channels of the Polrud River. (c,d) Longitudinal profile, Gd and Rd along Polrud River, and location of identified knickpoints.

near to one and equals 0.2 in the middle of the profile and at the bottom of the river where the Soheil fault is intersected, respectively (Figure 15a). A rapid change in concavity and gradient, where river branches cross Soheil, Deylaman and Samamous faults and an increase occurs in the magnitude of the normalized steepness, indicate that the basin has a high elevation while decreased erosion in the area (Figure 15b). Along the hanging wall of the Samamous fault, the local river reaches have  $K_{sn}$  values which increase to >100 (Figure 12b) and (Figure 15b). In addition, the maximum inclination of normalized steepness (245) is influenced by Soheil fault activity (Baharfirouzi et al. 2005) (Figure 15b). Further, the dip direction of the Deylaman fault is toward the north, and  $K_{sn}$  along the segment of the footwall of the fault is low although major increases in  $K_{sn}$  along the hanging wall are noted at the east end of the fault block (Figure 12c) and (Figure 15b). Furthermore, the Polrud River cut these structures and uplift the bedrock forming several knickpoints (Figure 15c,d).

Additionally, the Dohezar River in the Khashchal Mountain in sub-basin 35, which is located in the southeast of the study area, contains distinct knickpoints. In addition, this river cuts Kashachal and Nusha faults, and the cutting rate increases as moving downstream, increasing the magnitude of the normalized steepness to 273. The low erosion rate of river sediments in the upstream part of the river increased the amount of the concavity index (0.36) (Figure 16a) and produced different knickpoints with high elevations and relative steepness (Figure 16c). Further, the Safarud River in sub-basin 23 includes waterfalls and major knickpoints in the upstream (knickzones), and the normalized steepness index reaches up to a value of 274 at the intersection of the river with Khazar and Chalmehrud faults, which represents the recent tectonic activity of the Khazar fault and the increase in the uplift in this section. Furthermore, the high value of the concavity index (1.5) at the end of the river could be due to the loose and quaternary alluvium (Figure 16b). Additionally,  $K_{sn}$  increases toward the middle part of the footwall of the Chalmehrud fault (Figure 12b) and (Figure 16b). This fault at the confluence with the Safarud River in Javaherdeh village formed knickpoints and high altitude waterfalls, along with the knickzone of this section

(Figure 16d).

Knickpoints along the Chalakrud River (in the south of the study area) cut across Khazar, Soheil, and Nusha faults. The Khazar fault has an east-west bending direction and a dip direction toward the south and its function is inversely dip-slip (Fedynsky 1972). In addition,  $K_{sn}$  values in the hanging wall of the fault are mainly 50-100 and locally increase to >180 m of the fault. On the other hand, the lowest  $K_{sn}$  values reach along the coastline and the Khazar fault footwall, and the  $K_{sn}$  values for foot wall reaches are consistently low with a mean of <50 m (Figure 12a) and (Figure 17a). Further, the dextral strike-slip Nusha fault is located at the east end of the Kelishom fault (Berberian and Walker 2010), and the strike of the Nusha fault is northwest to the south-east and seems to dip toward the southwest (Hakimi Asiabar and Bagheriyan 2018). At the intersection of the Nusha fault with the river, the normalized steepness reached the highest value (380), indicating high tectonic activity. The river profile where the river crosses the Soheil fault has an extremely low concavity (0.18) (Figure 17b). Based on the findings, the knickpoints in the Chalakrud River formed with high altitudes indicate an increase in uplift and tectonic activity (Figure 17c,d).

Previous research on the characteristics of knickpoints demonstrates that knickpoints can be formed due to the performance of various forces such as hydrological process, lithological variations, and the active tectonic (Hayakawa and Oguchi 2006). Furthermore, knickpoints may be obvious waterfalls (e.g., Wohl et al. 1994; Hayakawa and Matsukura 2003). The obvious waterfall on the river in the upstream end of a large over the steepened zone can be due to regional or local tectonic processes (Reed and John 1981; Reneau 2000). The observation of knickpoints in the field and the laboratory analysis of knickpoints through GIS are analogous to each other (Figure 18).

#### 4 Conclusion

The study area is located in an active tectonic zone of Iran which is influenced by two important tectonic factors such as the Alborz uplift against the subsidence of the southern Caspian basin. Based

on the results, extremely high uplift rates had a clear effect on the morphology of the area. In addition, the uplift of the Alborz led to the increased elevation of basins, bed gradients, and

thus the incision rate of the stream channel. This increase in the gradient increased the flow strength into the bedrock beneath, and causes the channel to be cut and abrupt changes in paths. Further, the

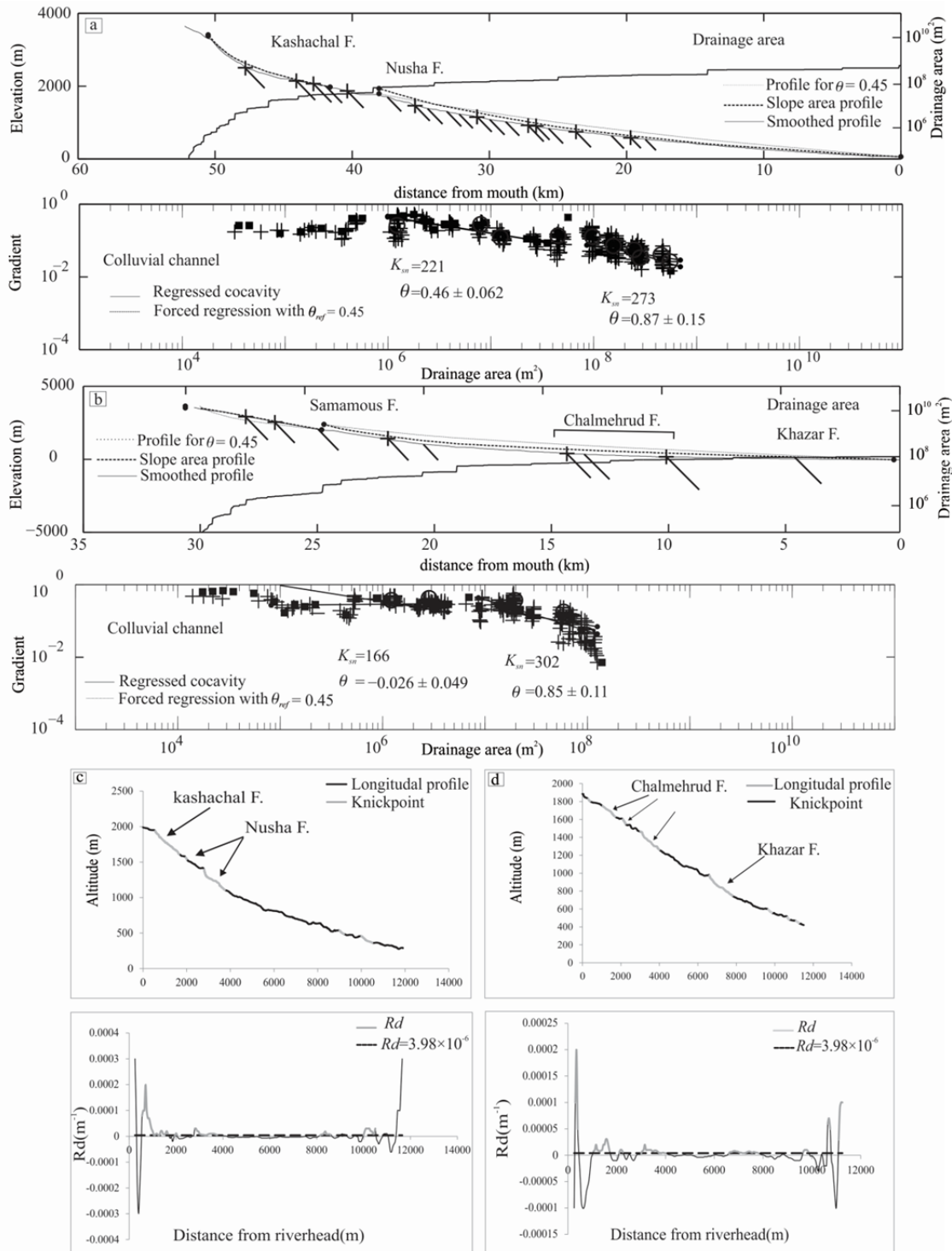


**Figure 16** (a,b) Longitudinal channel profiles and associated slope–area, log-log plots with best-fit regression lines defining concavity and gradient values for Dohezar River and Safarud River. (c,d) Longitudinal profile, Gd and Rd along for Dohezar River and Safarud River, and location of identified knickzones.



area is tectonically unstable based on the evidence of fault movements during the Quaternary. The obtained results suggest that the anomalously steep segments of the streams are mainly found along tectonic lineaments, and knickpoints identified

from the longitudinal profiles of rivers and field observations are comparable. Thus, the results confirmed that knickpoints or knickzones are useful in geomorphic interpretations. Furthermore, field results indicated that the structure is an

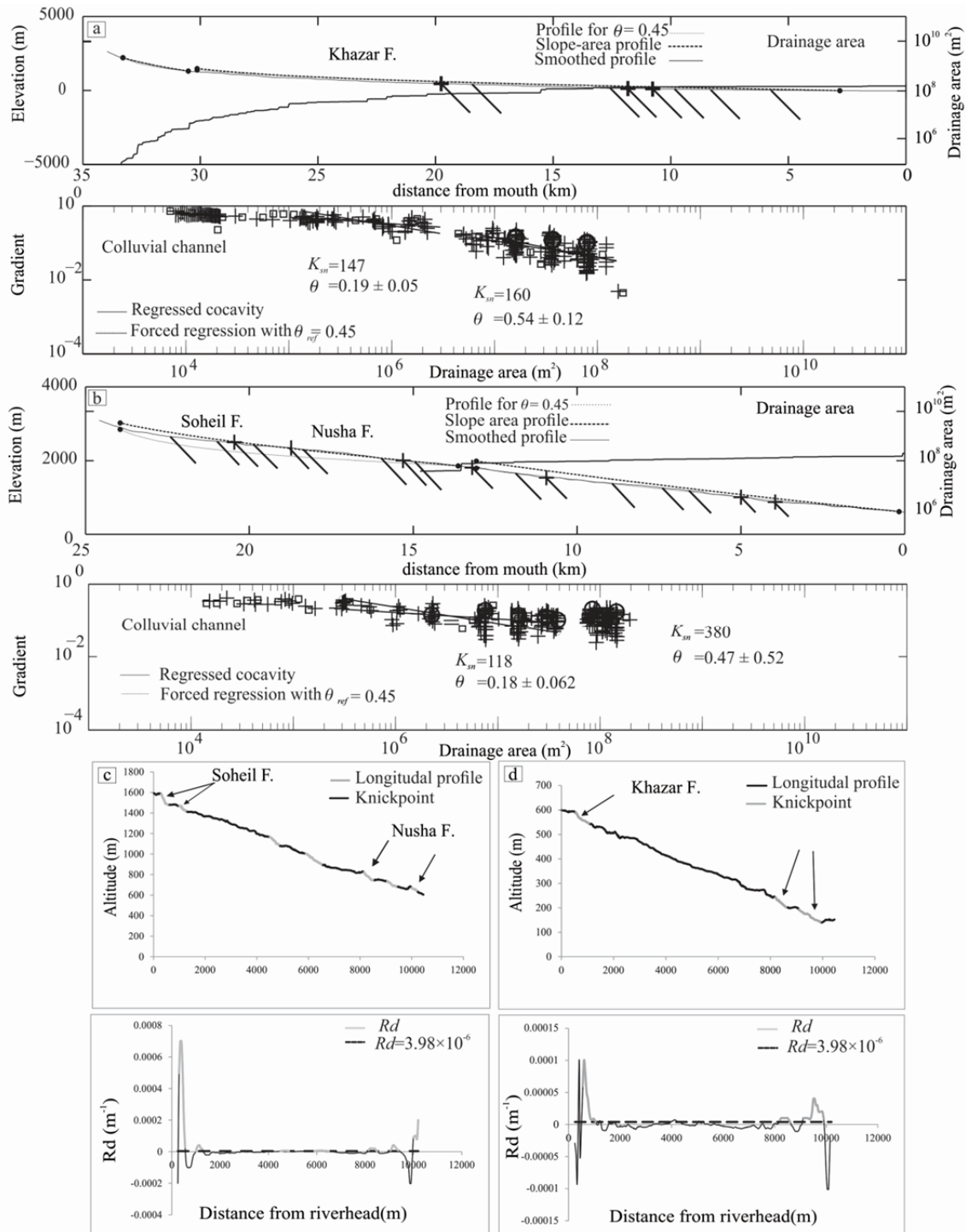


**Figure 17** (a,b) Longitudinal channel profiles and associated slope–area log-log plots with best-fit regression lines defining concavity and gradient values for the three studied channels of the Chalakrud River. (c,d) Longitudinal profile, Gd and Rd along Chalakrud River, and location of identified knickzones.



**Figure 18** (a) Waterfall a ~3 meters in the Polrud River corresponding to the Soheil fault near Kakrud village, Southwest view, (b) Waterfall, a~10 m at the Safarud River Knickzone corresponding to Chalmehrud fault Javaherdeh village, in the Northeast and North view, (c) The Knickpoint lithology at the Dohrzar River, North view (d) Waterfall a~10 meters in the Chalakrud River corresponding to the Deylaman fault, North view, (e) The Knickpoint in the Polrud River corresponding to the Khazar fault, Southeast view, (f) The Knickpoint lithology in the Polrud river, Northwest view.

important control affecting the knickpoint. In the present study, 150 major knickpoints were identified along the main rivers with more than 10-m in the study. Additionally, the results revealed

that major knickpoints of Polrud, Dohezar, Safarud and Chalakrud Rivers are associated with faults such as Khazar, Soheil, Zarrinrajeh, Kashachal Deylaman, Kelishom, Chalmehrud and Nusha which indeed present high  $K_{sn}$  and SL values therefore uplift of the hanging walls of these faults. Tectonic active landscapes such as gorges, elongated valleys, extensive deformations in Neogene and Quaternary units, Quaternary faulting, as well as different knickpoints and waterfalls along the rivers characterize the regional high topography. In addition, geomorphic indices demonstrated that the recent uplift is typical to the central part of main faults. Finally, the analysis of river profiles suggested that the topographic uplift is related to the high levels of the recent tectonic activity in the central and eastern parts of the study area. The results from the active tectonic parts of the region were related to active main faults while the value of the IAT index was extremely low in the northern and northeastern parts of the region including the coastal areas of the Caspian Sea in the footwall of the Khazar fault, indicating low tectonic activity and lower relief for the northern basins suggest relatively low uplift patterns in this area. Finally, the

obtained data indicated that the geomorphometric anomalies of drainage basins are considered as significant indicators of tectonic activity which can be used for studying seismic hazards in the future.

## References

- Aghanabati A (2004) Geology of Iran. Geological survey of Iran.
- Alavi, M (1996) Tectonostratigraphic synthesis and structural style of the Alborz mountain system in northern Iran. *Journal of Geodynamics* 21(1): 1-33.  
[https://doi.org/10.1016/0264-3707\(95\)00009-7](https://doi.org/10.1016/0264-3707(95)00009-7)
- Alexandrowicz Z (1994) Geologically controlled waterfall types in the Outer Carpathians. *Geomorphology* 9(2): 155-165.  
[https://doi.org/10.1016/0169-555X\(94\)90073-6](https://doi.org/10.1016/0169-555X(94)90073-6)
- Allen MB, Ghassemi MR, Shahrabi M, et al. (2003) Accommodation of late Cenozoic oblique shortening in the Alborz range, northern Iran. *Journal of structural geology* 25(5): 659-672.  
[https://doi.org/10.1016/S0191-8141\(02\)00064-0](https://doi.org/10.1016/S0191-8141(02)00064-0)
- Axen, G J, Lam PS, Grove M, et al. (2001) Exhumation of the west-central Alborz Mountains, Iran, Caspian subsidence, and collision-related tectonics. *Geology* 29(6): 559-562.  
[https://doi.org/10.1130/0091-7613\(2001\)029<0559:EOTWCA>2.0.CO;2](https://doi.org/10.1130/0091-7613(2001)029<0559:EOTWCA>2.0.CO;2)
- Baharfirozzi Kh, Shafeii AR, Azhdari A, et al. (2005) Geological map of Javaherdeh quadrangle, 1:100,000. Geological Survey

- of Iran, Tehran, Iran.
- Baker VR, Kale VS (1998) The role of in extreme floods shaping bedrock channels. *Geophysical Monograph-American Geophysical Geophysical Union* 107 (1): 153-166. <https://doi.org/10.1029/GM107p0153>
- Ballato P, Stockli DF, Ghassemi MR, et al. (2013). Accommodation of transpressional strain in the Arabia - Eurasia collision zone: New constraints from (U - Th)/He thermochronology in the Alborz mountains, north Iran. *Tectonics* 32(1): 1-18. <https://doi.org/10.1029/2012TC003159>
- Baroni, C, Noti, V, Ciccacci, S, et al. (2005) Fluvial origin of the valley system in northern Victoria Land (Antarctica) from quantitative geomorphic analysis. *Geological Society of America Bulletin* 117(1-2): 212-228. <https://doi.org/10.1130/B25529.1>
- Berberian M (1983) Generalized tectonic Map of Iran. Geological Survey of Iran Report No. 52.
- Berberian M, King GCP (1981) Towards a paleogeography and tectonic evolution of Iran. *Canadian journal of earth sciences* 18(11): 210-265. <https://doi.org/10.1139/e81-019>
- Berberian M, Yeats RS (1999) Patterns of historical earthquake rupture in the Iranian Plateau. *Bulletin of the Seismological society of America* 89(1):120-139. <https://doi.org/10.1016/B978-0-444-63292-0.00016-8>
- Berberian M, Walker R (2010) The Rudbār M w 7.3 earthquake of 1990 June 20; seismotectonics, coseismic and geomorphic displacements, and historic earthquakes of the western 'High-Alborz', Iran. *Geophysical Journal International* 182(3): 1577-1602. <https://doi.org/10.1111/j.1365-246X.2010.04705.x>
- Berberian M, Yeats RS (2001) Contribution of archaeological data to studies of earthquake history in the Iranian Plateau. *Journal of Structural Geology* 23(2-3): 563-584. [https://doi.org/10.1016/S0191-8141\(00\)00115-2](https://doi.org/10.1016/S0191-8141(00)00115-2)
- Bishop P, Goldrick, G (2010) Lithology and the evolution of bedrock rivers in post-orogenic settings: constraints from the high-elevation passive continental margin of SE Australia. *Geological Society, London, Special Publications* 346(1): 267-287. <https://doi.org/10.1144/SP346.0>
- Bishop P, Hoey TB, Jansen JD, et al. (2005) Knickpoint recession rate and catchment area: the case of uplifted rivers in Eastern Scotland. *Earth Surface Processes and Landforms: The Journal of the British Geomorphological Research Group* 30(6): 767-778. <https://doi.org/10.1130/B25529.1>
- Bozkurt E, Bozkurt E, Bozkurt JA, et al. (2000) Tectonics and magmatism in Turkey and the surrounding area. *Geological Society of London* 173(1): 385-403.
- Braga JC, Martín JM, Quesada C (2003) Patterns and average rates of late Neogene–Recent uplift of the Betic Cordillera, SE Spain. *Geomorphology* 50(1-3): 3-26. [https://doi.org/10.1016/S0169-555X\(02\)00205-2](https://doi.org/10.1016/S0169-555X(02)00205-2)
- Bull WB (1991) *Geomorphic responses to climatic change*. New York, Oxford University Press 326. <https://doi.org/10.1002/gea.3340080106>
- Bull WB (2009)a. *Tectonically Active Landscapes*. Wiley-Blackwell, Oxford 326.
- Bull WB, Mcfadden LD (1977) Tectonic geomorphology north and south of the Garlock fault, California. In *Geomorphology in Arid Regions, Proceeding 8th Annual Geomorphology Symposium, State University New York at Binghamton* 115-137.
- Burbank DW, Anderson RS (2001) *Tectonic geomorphology* John Wiley & Sons.
- Burk CA, Drake CL (eds.) (2013) *The geology of continental margins*. Springer.
- Cannon PJ, PJ C (1976) Generation of explicit parameters for a quantitative geomorphic study of Mill Creek drainage basin. *Oklahoma Geology Notes* 36 (1): 3-16.
- Chen YW, Shyu JBH, Chang CP (2015) Neotectonic characteristics along the eastern flank of the Central Range in the active Taiwan orogen inferred from fluvial channel morphology. *Tectonics* 34(10): 2249-2270. <https://doi.org/10.1002/2014TC003795>
- Ciccacci S, Fredi P, Lupia PE, et al. (1987). Indirect evaluation of erosion entity in drainage basins through geomorphic, climatic and hydrological parameters. In *International geomorphology, 1986: proceedings of the First International Conference on Geomorphology*. Chichester: Wiley.
- Crosby BT, Whipple KX (2006) Knickpoint initiation and distribution within fluvial networks: 236 waterfalls in the Waipaoa River, North Island, New Zealand. *Geomorphology* 82(1-2): 16-38. <https://doi.org/10.1016/j.geomorph.2005.08.023>
- Dewey JF, Hempton MR, Kidd WSF, et al. (1986) Shortening of continental lithosphere: the neotectonics of Eastern Anatolia—a young collision zone. *Geological Society, London, Special Publications* 19(1): 1-36. <https://doi.org/10.1144/GSL.SP.1986.019.01.01>
- DiBiase RA, Whipple KX, Heimsath AM, et al. (2010) Landscape form and millennial erosion rates in the San Gabriel Mountains, CA. *Earth and Planetary Science Letters* 289(1-2): 134-144. <https://doi.org/10.1016/j.epsl.2009.10.036>
- Duvall A, Kirby E, Burbank D (2004) Tectonic and lithologic controls on bedrock channel profiles and processes in coastal California. *Journal of Geophysical Research: Earth Surface* 109(F3). <https://doi.org/10.1029/2003JF000086>
- El Hamdouni R, Irigaray C, Fernández T, et al. (2008) Assessment of relative active tectonics, southwest border of the Sierra Nevada (southern Spain). *Geomorphology* 96(1-2), 150-173. <https://doi.org/10.1016/j.geomorph.2007.08.004>
- Fedynsky VV, KE F, JA G (1972). The Earth's crust of the inland seas and continental depressions of the west Tethys region.
- Flint JJ (1974) Stream gradient as a function of order, magnitude, and discharge. *Water Resources Research* 10(5): 969-973. <https://doi.org/10.1029/WR010i005p00969>
- Gallen SF, Pazzaglia FJ, Wegmann KW, et al. (2015) The dynamic reference frame of rivers and apparent transience in incision rates. *Geology* 43(7): 623-626. <https://doi.org/10.1130/G36692.1>
- Gardner TW (1983) Experimental study of knickpoint and longitudinal profile evolution in cohesive, homogeneous material. *Geological Society of America Bulletin* 94(5): 664-672. [https://doi.org/10.1130/0016-7606\(1983\)94<664:ESOKAL>2.0.CO;2](https://doi.org/10.1130/0016-7606(1983)94<664:ESOKAL>2.0.CO;2)
- García-Tortosa FJ, Alfaro P, Galindo-Zaldívar J, et al. (2008) Geomorphologic evidence of the active Baza fault (Betic Cordillera, south Spain). *Geomorphology* 97(3-4): 374-391. <https://doi.org/10.1016/j.geomorph.2007.08.007>
- Gasparini NM, Whipple KX (2014) Diagnosing climatic and tectonic controls on topography. Eastern flank of the northern Bolivian Andes. *Lithosphere* 6(4): 230-250. <https://doi.org/10.1130/L322.1>
- Ghassemi MR (2005) Drainage evolution in response to fold growth in the hanging-wall of the Khazar fault, north-eastern Alborz, Iran. *Basin Research* 17(3): 425-436. <https://doi.org/10.1111/j.1365-2117.2005.00271.x>
- Guarnieri P, Pirrotta C (2008) The response of drainage basins to the late Quaternary tectonics in the Sicilian side of the Messina Strait (NE Sicily). *Geomorphology* 260-273. <https://doi.org/10.1016/j.geomorph.2007.06.013>
- Guest B, Axen GJ, Lam PS, et al. (2006) Late Cenozoic shortening in the west-central Alborz Mountains, northern Iran, by combined conjugate strike-slip and thin-skinned deformation Geosphere: 35-52. <https://doi.org/10.1130/GES00019.1>
- Hack JT (1957) *Studies of longitudinal stream profiles in Virginia and Maryland* US Government Printing Office 294: 45-97.
- Hack JT (1973) Stream-profile analysis and stream-gradient index. *Journal of Research of the us Geological Survey* 421-429.
- Hack JT (1982) Physiographic divisions and differential uplift in the Piedmont and Blue Ridge No. 1265. USGPO.



- Hakimi Asiabar SH, Bagheriyan S (2018) Exhumation of the Deylaman fault trend and its effects on the deformation style of the western Alborz belt in Iran. *International Journal of Earth Sciences* 107(2): 539-551. <https://doi.org/10.1007/s00531-017-1507-4>
- Hancock GS, Anderson RS, Whipple KX (1998) Beyond power: Bedrock river incision process and form. *Geophysical Monograph-American Geophysical Union* 107: 35-60. <https://doi.org/10.1029/GM107p0035>
- Hayakawa Y, Matsukura Y (2003) Recesson rates of waterfalls in Boso Peninsula, Japan, and a predictive equation. *Earth Surface Processes and Landforms: The Journal of the British Geomorphological Research Group* 28(6): 675-684. <https://doi.org/10.1002/esp.519>
- Harkins NW, Anastasio DJ, Pazzaglia FJ (2005) Tectonic geomorphology of the Red Rock fault, insights into segmentation and landscape evolution of a developing range front normal fault. *Journal of Structural Geology* 1925-1939. <https://doi.org/10.1016/j.jsg.2005.07.005>
- Hayakawa YS, Oguchi T (2006) DEM-based identification of fluvial knickzones and its application to Japanese mountain rivers. *Geomorphology* 90-106. <https://doi.org/10.1016/j.geomorph.2006.01.018>
- Horton RE (1945) Erosional development of streams and their drainage basins; hydrophysical approach to quantitative morphology. *Geological society of America bulletin*. 56(3): 275-370. [https://doi.org/10.1130/0016-7606\(1945\)56\[275:EDOSAT\]2.o.CO;2](https://doi.org/10.1130/0016-7606(1945)56[275:EDOSAT]2.o.CO;2)
- Hovius N (2000) Macroscale process systems of mountain belt erosion. *Geomorphology and global tectonics* 77-105.
- Jackson J, Priestley K, Allen M, et al. (2002) Active tectonics of the south Caspian basin. *Geophysical Journal International* 214-245. <https://doi.org/10.1046/j.1365-246X.2002.01588.x>
- Johnson C (1997) Resolving denudational histories in orogenic belts with apatite fission-track thermochronology and structural data: An example from southern Spain. *Geology* 25(7): 623-626. [https://doi.org/10.1130/0091-7613\(1997\)025<0623:RDHIOB>2.3.CO;2](https://doi.org/10.1130/0091-7613(1997)025<0623:RDHIOB>2.3.CO;2)
- Keller EA (1986) Investigation of active tectonics: use of surficial earth processes. *Active tectonics* 136-147.
- Keller EA, Pinter N (1996) *Active tectonics Upper Saddle River, NJ: Prentice Hall* 19: 359.
- Keller EA, Pinter N (2002) Earthquakes, uplift, and landscape.
- Kirby E, Johnson C, Furlong K, et al. (2007) Transient channel incision along Bolinas Ridge, California: Evidence for differential rock uplift adjacent to the San Andreas Fault. *Journal of Geophysical Research: Earth Surface* 112(F3). <https://doi.org/10.1029/2006JF000559>
- Kirby E, Ouimet W (2011) Tectonic geomorphology along the eastern margin of Tibet: Insights into the pattern and processes of active deformation adjacent to the Sichuan Basin. *Geological Society, London, Special Publications* 353(1): 165-188. <https://doi.org/10.1144/SP353.9>
- Kirby E, Whipple KX (2001) Quantifying differential rock-uplift rates via stream profile analysis. *Geology* 29(5): 415-418. [https://doi.org/10.1130/0091-7613\(2001\)029<0415:QDRURV>2.o.CO;2](https://doi.org/10.1130/0091-7613(2001)029<0415:QDRURV>2.o.CO;2)
- Kirby E and Whipple KX (2012) Expression of active tectonics in erosional landscapes. *Journal of Structural Geology* 44: 54-75. <https://doi.org/10.1016/j.jsg.2012.07.009>
- Kirby E, Whipple KX, Tang W, et al. (2003) Distribution of active rock uplift along the eastern margin of the Tibetan Plateau: Inferences from bedrock channel longitudinal profiles. *Journal of Geophysical Research: Solid Earth* 108(B4). <https://doi.org/10.1029/2001JB000861>
- Kurtz R, Klinger Y, Ferry M, et al. (2018) Horizontal surface-slip distribution through several seismic cycles: The Eastern Bogd fault, Gobi-Altai, Mongolia. *Tectonophysics* 734: 167-182. <https://doi.org/10.1016/j.tecto.2018.03.011>
- Larue JP (2008) Effects of tectonics and lithology on long profiles of 16 rivers of the southern Central Massif border between the Aude and the Orb (France). *Geomorphology* 93(3-4). <https://doi.org/10.1016/j.geomorph.2007.03.003>
- Lavé J and Avouac JP (2001) Fluvial incision and tectonic uplift across the Himalayas of central Nepal. *Journal of Geophysical Research: Solid Earth* 106(B11): 26561-2659. <https://doi.org/10.1029/2001JB000359>
- Merritts D, Vincent KR (1989) Geomorphic response of coastal streams to low, intermediate, and high rates of uplift, Medocino triple junction region, northern California. *Geological Society of America Bulletin* 101(11): 1373-1388. [https://doi.org/10.1130/0016-7606\(1989\)101<1373:GROCST>2.3.CO;2](https://doi.org/10.1130/0016-7606(1989)101<1373:GROCST>2.3.CO;2)
- Merritts DJ, Vincent KR and Wohl EE (1994) Long river profiles, tectonism, and eustasy: A guide to interpreting fluvial terraces. *Journal of Geophysical Research: Solid Earth* 99(B7): 14031-14050. <https://doi.org/10.1029/94JB00857>
- Miller JR (1991) The influence of bedrock geology on knickpoint development and channel-bed degradation along downcutting streams in south-central Indiana. *The Journal of Geology* 99(4): 591-605. <https://doi.org/10.1086/629519>
- Moglen GE, Bras RL (1995) The importance of spatially heterogeneous erosivity and the cumulative area distribution within a basin evolution model. *Geomorphology* 12(3): 173-185. [https://doi.org/10.1016/0169-555X\(95\)00003-N](https://doi.org/10.1016/0169-555X(95)00003-N)
- Molin PAOLA, Fubelli GIANDOMENICO (2005) Morphometric evidence of the topographic growth of the Central Apennines. *Geografia Fisica e Dinamica Quaternaria* 28(3): 47-61.
- Ouimet WB, Whipple KX, Granger DE (2009) Beyond threshold hillslopes: Channel adjustment to base-level fall in tectonically active mountain ranges. *Geology*, 37(7), 579-582. <https://doi.org/10.1130/G30013A.1>
- Pederson, J.L, Tressler C (2012) Colorado River long-profile metrics, knickzones and their meaning. *Earth and Planetary Science Letters* 345: 171-179. <https://doi.org/10.1016/j.epsl.2012.06.047>
- PedrerA, Pérez-Peña JV, Galindo-Zaldívar J, et al. (2009) Testing the sensitivity of geomorphic indices in areas of low-rate active folding (eastern Betic Cordillera, Spain). *Geomorphology* 105(3-4): 218-231. <https://doi.org/10.1016/j.geomorph.2008.09.026>
- Pérez-Peña JV (2009) GIS-based tools and methods for landscape analysis and active tectonic evaluation.
- Pérez-Peña JV, Azor A, Azañón JM, et al. (2010) Active tectonics in the Sierra Nevada (Betic Cordillera, SE Spain): Insights from geomorphic indexes and drainage pattern analysis. *Geomorphology* 119(1-2): 74-87. <https://doi.org/10.1016/j.geomorph.2010.02.020>
- Pike RJ, Wilson SE (1971) Elevation-relief ratio, hypsometric integral, and geomorphic area-altitude analysis. *Geological Society of America Bulletin* 82(4): 1079-1084. [https://doi.org/10.1130/0016-7606\(1971\)82\[1079:ERHIAG\]2.o.CO;2](https://doi.org/10.1130/0016-7606(1971)82[1079:ERHIAG]2.o.CO;2)
- Rad FK (1986) A Jurassic delta in the eastern Alborz, NE Iran. *Journal of petroleum geology* 9(3): 281-294. <https://doi.org/10.1111/j.1747-5457.1986.tb00390.x>
- Ramírez - Herrera MT (1998) Geomorphic assessment of active tectonics in the Acambay Graben, Mexican volcanic belt. *Earth Surface Processes and Landforms: The Journal of the British Geomorphological Group* 23(4): 317-332. [https://doi.org/10.1002/\(SICI\)1096-9837\(199804\)23:4<317::AID-ESP845>3.o.CO;2-V](https://doi.org/10.1002/(SICI)1096-9837(199804)23:4<317::AID-ESP845>3.o.CO;2-V)
- Reed Jr, John C (1981). Disequilibrium profile of the Potomac River near Washington, DC—A result of lowered base level or Quaternary tectonics along the Fall Line? *Geology* 9(10): 445-450. [https://doi.org/10.1130/0091-7613\(1981\)9<445:DPOTPR>2.o.CO;2](https://doi.org/10.1130/0091-7613(1981)9<445:DPOTPR>2.o.CO;2)
- Reilinger R, McClusky S, Vernant P, et al. (2006) GPS constraints on continental deformation in the Africa - Arabia - Eurasia continental collision zone and implications for the dynamics of plate interactions. *Journal of Geophysical Research: Solid Earth* 111(B5).

- <https://doi.org/10.1029/2005JB004051>
- Reneau SL (2000) Stream incision and terrace development in Frijoles Canyon, Bandelier National Monument, New Mexico, and the influence of lithology and climate. *Geomorphology* 32(1-2): 171-193. [https://doi.org/10.1016/S0169-555X\(99\)00094-X](https://doi.org/10.1016/S0169-555X(99)00094-X)
- Ritz J F, Nazari H, Ghassemi A, et al. (2006) Active transtension inside central Alborz: A new insight into northern Iran-southern Caspian geodynamics. *Geology* 34(6): 477-480. <https://doi.org/10.1130/G22319.1>
- Rockwell TK, Keller EA, Johnson DL (1985) Tectonic geomorphology of alluvial fans and mountain fronts near Ventura, California. In *Tectonic Geomorphology. Proceedings of the 15th Annual Geomorphology Symposium*. Allen and Unwin Publishers, Boston, MA 183-207.
- Safran EB, Bierman PR, Aalto R, et al. (2005) Erosion rates driven by channel network incision in the Bolivian Andes. *Earth Surface Processes and Landforms: The Journal of the British Geomorphological Research Group* 30(8): 1007-1024. <https://doi.org/10.1002/esp.1259>
- Schumm SA (1956) Evolution of drainage systems and slopes in badlands at Perth Amboy. *New Jersey, Geological society of America bulletin* 67(5): 597-646. [https://doi.org/10.1130/0016-7606\(1956\)67\[597:EODSAS\]2.o.CO;2](https://doi.org/10.1130/0016-7606(1956)67[597:EODSAS]2.o.CO;2)
- Schumm SA, Schumm SA, Dumont JF, et al. (2002) *Active tectonics and alluvial rivers*. Cambridge University Press.
- Schumm SA (2007) *River variability and complexity*. Cambridge University Press.
- Seeber L, Gornitz V (1983) River profiles along the Himalayan arc as indicators of active tectonics. *Tectonophysics* 92(4): 335-367. [https://doi.org/10.1016/0040-1951\(83\)90201-9](https://doi.org/10.1016/0040-1951(83)90201-9)
- Shahzad F, Mahmood SA, Gloaguen R (2009) Drainage network and lineament analysis: an approach for Potwar Plateau (northern Pakistan). *Journal of Mountain Science* 6(1): 14. <https://doi.org/10.1007/s11629-009-0206-4>.
- Sharma G, Mohanty S (2018) Morphotectonic analysis and GNSS observations for assessment of relative tectonic activity in Alaknanda basin of Garhwal Himalaya. *India. Geomorphology* 301: 108-120. <https://doi.org/10.1016/j.geomorph.2017.11.002>
- Slingerland R, Willett SD, Hovius N (1998) Slope-area scaling as a test of fluvial bedrock erosion laws. *Eos Trans. AGU* 79(45).
- Snyder NP, Whipple KX, Tucker GE, et al. (2000) Landscape response to tectonic forcing: Digital elevation model analysis of stream profiles in the Mendocino triple junction region, northern California. *Geological Society of America Bulletin* 112(8): 1250-1263. [https://doi.org/10.1130/0016-7606\(2000\)112<1250:LRTTFD>2.o.CO;2](https://doi.org/10.1130/0016-7606(2000)112<1250:LRTTFD>2.o.CO;2)
- Stahler A (1952) Hypsometric (area altitude) analysis of erosional topology. *Geol Soc Am Bull* 63: 1117-1142. [https://doi.org/10.1130/0016-7606\(1952\)63\[1117:HAAOET\]2.o.CO;2](https://doi.org/10.1130/0016-7606(1952)63[1117:HAAOET]2.o.CO;2)
- Stampfli G, Marcoux J, Baud A (1991) Tethyan margins in space and time. *Palaeogeography, Palaeoclimatology, Palaeoecology* 87(1-4): 373-409. [https://doi.org/10.1016/0031-0182\(91\)90142-E](https://doi.org/10.1016/0031-0182(91)90142-E)
- Stocklin J (1968) Structural history and tectonics of Iran: a review. *AAPG bulletin* 52(7): 1229-1258.
- Tatar M, Jackson J, Hatzfeld D, et al. (2007) The 2004 May 28 Baladeh earthquake (M w 6.2) in the Alborz, Iran: overthrusting the South Caspian Basin margin, partitioning of oblique convergence and the seismic hazard of Tehran. *Geophysical Journal International* 170(1): 249-261. <https://doi.org/10.1111/j.1365-246X.2007.03386.x>
- Tarboton DG, Bras RL, Rodriguez - Iturbe I (1991) On the extraction of channel networks from digital elevation data. *Hydrological processes* 5(1) 81-100. <https://doi.org/10.1002/hyp.3360050107>
- VanLaningham S, Meigs A, Goldfinger C (2006) The effects of rock uplift and rock resistance on river morphology in a subduction zone forearc, Oregon, USA. *Earth Surface Processes and Landforms: The Journal of the British Geomorphological Research Group* 31(10): 1257-1279. <https://doi.org/10.1002/esp.1326>
- Vernant P, Nilforoushan F, Chery J, et al. (2004) Deciphering oblique shortening of central Alborz in Iran using geodetic data. *Earth and Planetary Science Letters* 223(1-2): 177-185. <https://doi.org/10.1016/j.epsl.2004.04.017>
- Whipple KX (2004) Bedrock rivers and the geomorphology of active orogens. *Annu. Rev. Earth Planet Sci* 32: 151-185. <https://doi.org/10.1146/annurev.earth.32.101802.120356>
- Whipple KX, Tucker GE (2002) Implications of sediment - flux - dependent river incision models for landscape evolution. *Journal of Geophysical Research: Solid Earth* 107(B2): ETG-3. <https://doi.org/10.1029/2001JB000162>
- Whipple KX, Tucker GE (1999) Dynamics of the stream - power river incision model: Implications for height limits of mountain ranges, landscape response timescales, and research needs. *Journal of Geophysical Research: Solid Earth* 104(B8): 17661-17674. <https://doi.org/10.1029/1999JB900120>
- Whipple KX, Dibiase RA, Crosby BT (2013) Bedrock rivers. In *Treatise on geomorphology* 550-573. <https://doi.org/10.1016/B978-0-12-374739-6.00254-2>
- Willgoose G, Bras RL, Rodriguez - Iturbe I (1990) A model of river basin evolution. *Eos. Transactions American Geophysical Union* 71(47):1806-1807. <https://doi.org/10.1029/90EO00349>
- Wobus C, Whipple KX, Kirby E, et al. (2006) Tectonics from topography: Procedures, promise, and pitfalls. *Special papers-geological society of America* 398: 55. [https://doi.org/10.1130/2006.2398\(04\)](https://doi.org/10.1130/2006.2398(04))
- Wohl EE, Greenbaum N, Schick AP and Baker VR (1994) Controls on bedrock channel incision along Nahal Paran, Israel. *Earth Surface Processes and Landforms* 19(1): 1-13. <https://doi.org/10.1002/esp.3290190102>
- Zanchi A, Berra F, Mattei M, et al. (2006) Inversion tectonics in central Alborz, Iran. *Journal of Structural Geology* 28(11): 2023-2037. <https://doi.org/10.1016/j.jsg.2006.06.020>